nature medicine

Microenvironmental control of breast cancer subtype elicited through paracrine platelet-derived growth factor-CC signaling

Pernilla Roswall[1,2,11], Matteo Bocci[1,11], Michael Bartoschek[1,11], Hong Li[2,11], Glen Kristiansen[3], Sara Jansson[4], Sophie Lehn[1], Jonas Sjölund[1], Steven Reid[1], Christer Larsson[1], Pontus Eriksson[4], Charlotte Anderberg[1], Eliane Cortez[1], Lao H Saal[4], Christina Orsmark-Pietras[5], Eugenia Cordero[1], Bengt Kristian Haller[2], Jari Häkkinen[4], Ingrid J G Burvenich[6], Elgene Lim[7,8], Akira Orimo[9], Mattias Höglund[4], Lisa Rydén[4], Holger Moch[10], Andrew M Scott[6], Ulf Eriksson[2] & Kristian Pietras[1]

Breast tumors of the basal-like, hormone receptor–negative subtype remain an unmet clinical challenge, as there is high rate of recurrence and poor survival in patients following treatment. Coevolution of the malignant mammary epithelium and its underlying stroma instigates cancer-associated fibroblasts (CAFs) to support most, if not all, hallmarks of cancer progression. Here we delineate a previously unappreciated role for CAFs as determinants of the molecular subtype of breast cancer. We identified paracrine crosstalk between cancer cells expressing platelet-derived growth factor (PDGF)-CC and CAFs expressing the cognate receptors in human basal-like mammary carcinomas. Genetic or pharmacological intervention of PDGF-CC activity in mouse models of cancer resulted in conversion of basal-like breast cancers into a hormone receptor-positive state that enhanced sensitivity to endocrine therapy in previously resistant tumors. We conclude that specification of breast cancer to the basal-like subtype is under microenvironmental control and is therapeutically actionable.

Breast cancer is a heterogeneous disease that manifests as a range of different molecular subtypes of clinical relevance, which can be identified through gene expression analyses or biomarker expression[1,2]. Breast tumors of the luminal subtypes (A or B) account for 70% of all mammary carcinomas and are characterized by expression of hormone receptors for estrogen (estrogen receptor α (ERα)) and/or progesterone (PgR), whereas 10–15% of women carry tumors of the basal-like subtype that do not express hormone receptors[3]. The prognosis and predictive characteristics of each breast cancer subtype are reflected by the adjuvant therapy options that are offered for a particular group of patients[4–6]. Patients carrying luminal tumors typically benefit from treatment with drugs that impinge on ERα signaling, such as tamoxifen, fulvestrant or aromatase inhibitors[7]. In contrast, out of all breast carcinomas, basal-like tumors have the highest recurrence rate, the shortest time to recurrence and the worst overall survival rate owing to a paucity of therapeutic targets[1,3,8,9]. Thus, new treatment approaches for patients with basal-like breast cancer are urgently required.

Breast cancer subtypes are defined according to the characteristics of the malignant cells in the tumor. However, this tumor cell–centric view does not take into account the context in which cancer cells subsist. As the cancerous lesion progresses, the surrounding microenvironment coevolves into an activated state through continuous paracrine communication, thus creating a dynamic signaling circuitry that promotes malignant initiation and progression[10]. Hence, from a therapeutic perspective, tumors must be regarded as multicellular organs. CAFs are a major constituent cell type of tumor stroma and are known to support many different aspects of tumor growth and progression through secretion of growth-stimulatory, angiogenic, immune-modulatory and proinvasive factors[11,12]. However, the potential for CAFs as therapeutic targets or as prognostic and/or predictive biomarkers is still under debate, opening the possibility that CAFs represent a heterogeneous group of cells with diverse and opposing functions[13,14]. Indeed, a recent study defined histological subtypes of the fibroblastic stroma of breast carcinomas on the basis of morphological criteria and marker expression[15].

We have previously demonstrated a role for signaling through PDGFs in the recruitment and functionality of CAFs in solid tumors, such as melanoma and cervical carcinoma[16,17]. Although CAFs have been reported to express both PDGF receptors, i.e., PDGFR-α and

[1]Division of Translational Cancer Research, Department of Laboratory Medicine, Lund University, Lund, Sweden. [2]Division of Vascular Biology, Department of Medical Biochemistry and Biophysics, Karolinska Institutet, Stockholm, Sweden. [3]Institute of Pathology, University Hospital Bonn, Bonn, Germany. [4]Division of Oncology and Pathology, Department of Clinical Sciences, Lund University, Lund, Sweden. [5]Division of Clinical Genetics, Department of Laboratory Medicine, Lund University, Lund, Sweden. [6]Olivia Newton-John Cancer Research Institute and School of Cancer Medicine, La Trobe University, Melbourne, Victoria, Australia. [7]Garvan Institute of Medical Research, Sydney, New South Wales, Australia. [8]University of New South Wales, Sydney, New South Wales, Australia. [9]Department of Pathology and Oncology, Juntendo University School of Medicine, Tokyo, Japan. [10]Department of Pathology and Molecular Pathology, University Hospital Zürich, Zürich, Switzerland. [11]These authors contributed equally to this work. Correspondence should be addressed to K.P. (kristian.pietras@med.lu.se).

Received 11 July 2016; accepted 12 January 2018; published online 12 March 2018; doi:10.1038/nm.4494

PDGFR-β, signaling pathway activity is determined through the preferential activation of these receptors via the five different PDGF ligand isoforms (PDGF-AA, PDGF-AB, PDGF-BB, PDGF-CC and PDGF-DD). The *in vivo* specificity of one of these PDGF isoforms, PDGF-CC, remains undetermined, although *in vitro* studies suggest that PDGF-CC may activate PDGF receptor alpha (PDGFR-α) homodimers as well as PDGFR-α/β heterodimers[18,19]. Herein, we delineate a previously unappreciated role for paracrine signaling through PDGF-CC in CAFs in the specification of the molecular subtype of breast cancer, which is a determinant of patient prognosis and treatment response. In several large and well-characterized cohorts of patients with breast cancer, we found that PDGF-CC expression in the malignant epithelium of breast cancer was associated with a hormone receptor–negative state. Genetic or pharmacological targeting of PDGF-CC in experimental mouse models resulted in conversion of basal-like breast tumors into an ERα-positive state that conferred sensitivity to endocrine therapy in previously resistant tumors. Our work sheds light on previously unknown mechanisms that define breast cancer subtype and has significant therapeutic implications for patients with basal-like breast tumors.

RESULTS

PDGF-CC is an independent prognostic factor for poor survival in breast cancer

To investigate the expression pattern of PDGF-CC in human breast cancer, we performed immunostaining of a tissue microarray containing 890 tumor specimens as well as healthy breast tissues (The Zurich cohort[20]; for patient characteristics, see **Supplementary Table 1**). Expression of PDGF-CC in healthy breast tissue was limited to basal myoepithelial cells and endothelial cells in capillaries, whereas PDGF-CC expression was not detected in luminal epithelial cells (**Fig. 1a**,**b**). In breast tumors, PDGF-CC was expressed by malignant cells, intratumoral capillaries and stromal fibroblasts (**Fig. 1c**). Notably, PDGF-CC immunoreactivity was most conspicuous at the border between stromal tissue and malignant epithelium (**Fig. 1d**). Next, we evaluated the staining intensity for PDGF-CC in the independent epithelial and stromal compartments (for scoring schemes, see **Supplementary Fig. 1a**,**b**) and correlated these findings to clinicopathological parameters. Both stromal and malignant epithelial expression of PDGF-CC was positively correlated to the grade and proliferative index of the tumor, but not to the stage or lymph node status (**Supplementary Table 2**). Stromal immunoreactivity for PDGF-CC was neither associated with patient outcome in Kaplan–Meier survival analysis nor identified as a risk factor for poor survival in univariate Cox regression analysis (**Supplementary Fig. 1c** and **Table 1**). In contrast, moderate to high expression of PDGF-CC in malignant cells (score of 1+ to 3+) was found to be a statistically significant prognostic factor for poor survival (**Fig. 1e** and **Table 1**). Notably, multivariable Cox regression analysis adjusted for established clinical risk factors, such as age at diagnosis, stage, grade, lymph node status and hormone receptor expression among others, demonstrated that epithelial expression of PDGF-CC served as an independent prognostic factor for poor survival in breast cancer (**Table 1**).

Our findings were corroborated in a second cohort of 550 patients with breast cancer (the Lund cohort[21,22]; for patient characteristics see **Supplementary Table 3**), in which high epithelial expression of PDGF-CC was correlated with tumor grade and associated with poor survival (**Supplementary Table 4** and **Supplementary Fig. 1d**). Both receptors in the PDGF family, i.e., PDGFR-α and PDGFR-β, were prominently and uniformly expressed by stromal fibroblasts in tumors from the Lund cohort (**Supplementary Fig. 1e**,**f**; PDGFR-α and PDGFR-β were expressed by CAFs in 482 of 489 (98.6%) and 480 of 480 (100%) of evaluable tumors, respectively). These findings indicate that malignant cells engage in functional paracrine communication with mesenchymal cells of the tumor microenvironment through PDGF signaling.

PDGF-CC is functionally important for growth of experimental breast cancer *in vivo*

To investigate the functional aspects of PDGF-CC expression in the context of mammary gland tumorigenesis, we generated a genetically engineered mouse model of breast cancer based on the widely studied and relevant MMTV-PyMT mouse[23,24] intercrossed with mice carrying an insertion of a lacZ cassette that inactivates the gene encoding PDGF-CC[25] (*Pdgfc*$^{-/-}$ mice). Visualization of PDGF-CC, PDGFR-α and PDGFR-β expression in tumors of MMTV-PyMT mice demonstrated consistent recapitulation of the expression pattern seen in human breast cancers, thus establishing the existence of a paracrine PDGF circuitry between malignant cells and stromal fibroblasts (**Supplementary Fig. 2a–d**). Strikingly, genetic deficiency for *Pdgfc* severely impacted the growth of mammary tumors in MMTV-PyMT mice (**Fig. 1f**). Control mice presented with tumors of an average size of 220 ± 47 mm^3 (mean ± s.e.m.), whereas deficiency for a single copy or both copies of the *Pdgfc* allele significantly reduced the average tumor size to 96 ± 41 mm^3 and 87 ± 71 mm^3, respectively (**Fig. 1f**). Genetic deficiency for *Pdgfc* was also associated with a significantly longer tumor latency as well as prolonged survival of the mice (**Supplementary Fig. 3a**,**b**). In line with the findings in human breast cancer, histological analyses revealed that tumors from *Pdgfc*$^{-/-}$ mice were of a lower grade than tumors from age-matched control mice (**Fig. 1g–i**) and had significantly larger areas of necrosis (**Fig. 1g**,**j**,**k**). We also observed a trend toward fewer pulmonary metastases in the absence of PDGF-CC signaling in 14-week-old tumor-bearing mice (**Supplementary Fig. 3c**). However, this was most likely due to the delayed onset of disease, as a cohort of wild-type (WT) mice with tumors that were grade-matched to those of the *Pdgfc*$^{-/-}$cohort displayed a similar metastatic burden as the mice lacking *Pdgfc* (**Supplementary Fig. 3c**).

To determine that the delayed tumor development in *Pdgfc*$^{-/-}$ mice was not due to developmental defects, we transplanted fragments of tumors from MMTV-PyMT; *Pdgfc*$^{+/+}$ and MMTV-PyMT; *Pdgfc*$^{-/-}$ mice orthotopically into the mammary fat pads of nontransgenic FVB/n mice. Whereas all transplanted *Pdgfc*$^{+/+}$ tumor fragments (21 of 21) established as growing tumors, only about half of the transplanted fragments from *Pdgfc*$^{-/-}$ mice (11 of 21; χ^2 test, $P = 0.003$) gave rise to tumors. In accordance with our findings in the transgenic setting, growth of the transplanted *Pdgfc*$^{-/-}$ tumors was dramatically hampered as compared to that of the *Pdgfc*$^{+/+}$ tumors (**Fig. 1l**). In addition, whereas two independently isolated cell lines derived from tumors in WT MMTV-PyMT mice (PeRo-Bas1 and PeRo-Bas2 cells) readily gave rise to tumors that grew exponentially following orthotopic transplantation into the mammary fat pads of FVB/n mice, cell lines from tumors derived from MMTV-PyMT; *Pdgfc*$^{-/-}$ mice (PeRo-Lum1 cells and PeRo-Lum2 cells) failed to efficiently establish as palpable tumors (**Supplementary Fig. 3d**,**e**).

Pdgfc deficiency results in a blunted fibrotic and angiogenic response in the tumor microenvironment

Histological analyses revealed considerable differences in tumor architecture between MMTV-PyMT; *Pdgfc*$^{+/+}$ and MMTV-PyMT; *Pdgfc*$^{-/-}$ mice. Masson's trichrome staining of tumor sections demonstrated

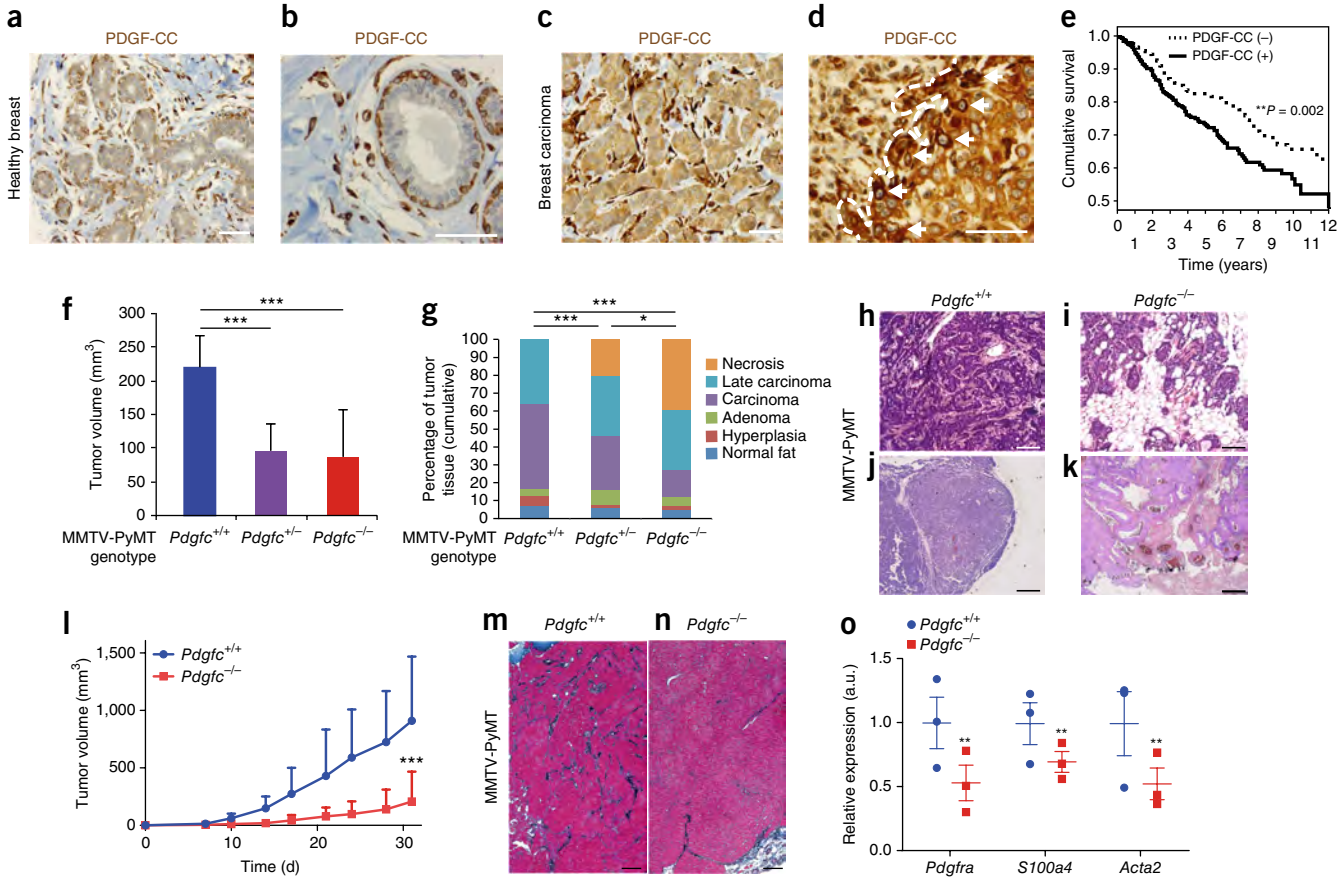

Figure 1 Epithelial expression of PDGF-CC is associated with a poor outcome in patients with breast carcinoma. (**a**–**d**) Immunostaining of healthy breast tissue (**a**,**b**) or breast carcinoma (**c**,**d**) for PDGF-CC. Results were validated on >10 independent samples to ensure the staining pattern on human tissue was reproducible. The dashed line represents the epithelium–stroma boundary, and arrows identify tumor cells with particularly high expression of PDGF-CC on the invasive border. Scale bars, 40 μm. (**e**) Kaplan–Meier analysis of breast cancer–specific survival dichotomized according to absence (negative; $n = 438$ samples) or presence (positive, defined as a score of 1+ to 3+; $n = 452$ samples) of PDGF-CC in tumor cells (for scoring scheme, see **Supplementary Fig. 1a**) of individuals with breast carcinomas from the Zürich cohort. $^{**}P = 0.002$; log-rank test. (**f**) Average volume (with s.e.m.) of tumors from 14-week-old MMTV-PyMT mice ($n = 10$ mice in each group). $^{***}P = 0.0001$; two-sided, unpaired, equal variance Student's *t*-test. (**g**) Grading of tumors from 14-week-old MMTV-PyMT mice ($n = 5$ mice in each group). $^{*}P = 0.036$; distribution of *Pdgfc*$^{-/-}$ versus *Pdgfc*$^{+/-}$, χ^2 test. $^{***}P = 3 \times 10^{-11}$; distribution of *Pdgfc*$^{-/-}$ versus *Pdgfc*$^{+/+}$, χ^2 test. $^{***}P = 0.00052$; distribution of *Pdgfc*$^{+/-}$ versus *Pdgfc*$^{+/+}$, χ^2 test. (**h**–**k**) H&E staining of tumors from *Pdgfc*$^{+/+}$ (**h**,**j**) and *Pdgfc*$^{-/-}$ (**i**,**k**) MMTV-PyMT mice at 14 weeks of age. Images shown are from one tumor of each genotype, but is representative of analysis of 5 mice per group. Scale bars, 500 μm. (**l**) Average volume (with s.e.m.) of tumors derived from MMTV-PyMT mice transplanted into the mammary fat pad of WT mice ($n = 21$ mice in each group, comprising $n = 7$ mice from 3 independent experiments for each group). $^{***}P = 6 \times 10^{-6}$; two-sided, unpaired, equal variance Student's *t*-test. (**m**,**n**) Masson's trichrome staining of tissue sections from tumors from 14-week-old *Pdgfc*$^{+/+}$ (**m**) and *Pdgfc*$^{-/-}$ (**n**) MMTV-PyMT mice. Stains are representative of $n = 10$ mice from each group. Scale bars, 500 μm. (**o**) Results from qRT-PCR analysis showing the average expression (with s.e.m.) of markers for cancer-associated fibroblasts in tumor lysates of tumors from 14-week-old MMTV-PyMT mice ($n = 3$ mice in each group; analysis was performed independently 3 times). a.u., arbitrary units. $^{**}P = 0.007$ (*Pdgfra*), $P = 0.003$ (*S100a4*), $P = 0.009$ (*Acta2*); two-sided, unpaired, equal variance Student's *t*-test.

a severely reduced deposition of intratumoral collagen in the matrix of *Pdgfc*$^{-/-}$ tumors, which is consistent with the notion that PDGF-CC signaling promotes the recruitment and/or activation of stromal fibroblasts in the breast tumor microenvironment (**Fig. 1m**,**n**). In support of this idea, qRT-PCR analysis showed a reduced abundance of mRNA transcripts of genes encoding prototypical markers for CAFs, such as α-smooth muscle actin (*Acta2*), fibroblast-specific protein 1 (*S100a4*) and PDGFR-α (*Pdgfra*), in *Pdgfc*$^{-/-}$ tumor samples (**Fig. 1o**; Student's *t*-test, $P < 0.01$ for each marker). Tumors from MMTV-PyMT; *Pdgfc*$^{-/-}$ mice exhibited significantly increased levels of hypoxia, as evidenced through immunostaining for HIF-1α, the master transcriptional regulator of hypoxia (**Supplementary Fig. 4a**–**c**). In accordance, qRT-PCR analysis revealed a 65% reduction in levels of vascular endothelial growth factor-A expression in the absence of PDGF-CC (**Supplementary Fig. 4d**). Furthermore, in line with the increased abundance of necrotic area, these tumors were severely hemorrhagic (**Supplementary Fig. 4e**). Neutralization of PDGF-CC through administration of the inhibitory antibody 6B3 in tumor-bearing SCID mice delayed the growth and angiogenic response of orthotopic basal-like MDA-MB-231 tumors (**Supplementary Fig. 5a**–**c**). Taken together, these results from genetic and pharmacological blockade of PDGF-CC corroborate a role for paracrine signaling in breast tumor growth, CAF recruitment and angiogenesis.

Expression of PDGF-CC in breast tumors is associated with a basal-like molecular subtype

To elucidate the molecular signature of *Pdgfc*-deficiency, we performed transcriptional analysis of tumors derived from MMTV-PyMT;

Table 1 Cox regression analysis of risk factors for breast cancer death in the Zurich cohort

	Univariable analysis		Multivariable analysis	
Parameter	RR (95% CI)	*P* value	RR (95% CI)	*P* value
Age at diagnosis				
<60 years vs. ≥60 years	1.542 (1.170–2.032)	0.002	1.437 (1.035–1.995)	0.03
Menopausal status				
pre- vs. post-	1.355 (0.965–1.902)	0.079	NA	NA
pT				
1–4	1.611 (1.421–1.825)	<0.001	1.624 (1.378–1.913)	<0.001
pN				
0–3	1.681 (1.423–1.986)	<0.001	1.415 (1.173–1.708)	<0.001
G				
1–3	1.669 (1.341–2.077)	<0.001	1.410 (1.067–1.862)	0.016
ERα				
negative vs. positive	0.494 (0.364–0.670)	<0.001	1.211 (0.757–1.937)	0.424
PgR				
negative vs. positive	0.511 (0.388–0.673)	<0.001	0.603 (0.411–0.886)	0.01
HER2				
0–2+ vs. 3+	1.941 (1.373–2.745)	<0.001	1.577 (1.041–2.388)	0.031
CK5/6				
negative vs. positive	1.496 (1.010–2.217)	0.045	1.457 (0.891–2.382)	0.133
PDGF-CC epithelium				
0 vs. 1–3+	1.520 (1.156–1.998)	0.003	1.484 (1.035–2.127)	0.032
PDGF-CC stroma				
1+ vs. 2+, 3+	0.931 (0.708–1.225)	0.931	NA	NA

RR, relative risk; CI, confidence interval; NA, not analyzed; pT, primary tumor stage; pN, number of lymph nodes involved; G, Nottingham histological grade; CK5/6, cytokeratin 5/6.

Pdgfc$^{+/+}$ and MMTV-PyMT; *Pdgfc*$^{-/-}$ mice using a qRT-PCR array designed to analyze a targeted panel of genes that are instrumental in breast tumor development and progression. The most differentially regulated gene was found to be forkhead box A1 (*Foxa1*); its expression was, on average, 17.2-fold higher in whole-tumor lysates from MMTV-PyMT; *Pdgfc*$^{-/-}$ mice than in MMTV-PyMT; *Pdgfc*$^{+/+}$ mice and 6.5-fold higher in cell lines isolated from *Pdgfc*$^{-/-}$ tumors than in *Pdgfc*$^{+/+}$ tumors (**Fig. 2a** and **Supplementary Fig. 6a**). The association between FOXA1 expression and loss of PDGF-CC was further corroborated at the protein level in whole-tumor lysates of mammary carcinomas from MMTV-PyMT; *Pdgfc*$^{+/-}$ mice and MMTV-PyMT; *Pdgfc*$^{-/-}$ mice (**Supplementary Fig. 6b**).

Next, we set out to determine the functional implications of high expression of *Foxa1* in breast tumors from *Pdgfc*$^{-/-}$ mice. Analysis of the transcriptional profiles of 1,086 breast tumors collected within The Cancer Genome Atlas (TCGA) network[26] revealed that expression of *FOXA1* was highly correlated with a non-basal-like molecular subtype (**Supplementary Fig. 6c**), confirming results from previous studies[1,27,28]. In accordance with the association between *FOXA1* and breast cancer of the luminal subtype, tumors from MMTV-PyMT; *Pdgfc*$^{-/-}$ mice with high levels of FOXA1 protein also exhibited robust expression of ERα, as determined through western blot analysis (**Supplementary Fig. 6b**). Considering the fact that *Foxa1* was found to be upregulated in mouse models of breast cancer in the absence of *Pdgfc*, we investigated the correlation between *FOXA1* and *PDGFC* in human breast cancer. Transcriptional data mined from a panel of 51 breast tumor–derived cell lines[29] revealed that expression of *FOXA1* was a specific feature of cell lines of the luminal subtype, whereas basal-like cell lines did not express meaningful levels of *FOXA1*, as expected (**Fig. 2b**). In contrast, high expression of *PDGFC* was predominantly observed in breast tumor cell lines of the basal-like subtype but not in cells originating from the luminal subtype (**Fig. 2c**). Indeed, the expression of *PDGFC* exhibited a statistically significant inverse correlation with that of *FOXA1* in this panel of cell lines (**Fig. 2d**). The enrichment for expression was exclusively observed for *PDGFC* and not for other members of the PDGF family in cell lines derived from basal-like breast tumors (**Fig. 2e**). We next investigated whether the absence of *PDGFC* was associated with a genome-wide regulatory gene program signifying luminal breast tumors. Using public data sets from chromatin immunoprecipitation and sequencing (ChIP–seq) analyses of luminal MCF7 and T47D cells[30], we analyzed the enrichment of binding sites for the luminal-defining transcription factors encoded by estrogen receptor 1 (*ESR1*), *FOXA1*, and GATA binding protein 3 (*GATA3*) in the genes most differentially expressed between estradiol (E2)-stimulated *Pdgfc*$^{-/-}$ PeRo-Lum1 cells and *Pdgfc*$^{+/+}$ PeRo-Bas1 cells. Although we were unable to demonstrate further induction of expression of *Esr1*-target genes following E2 stimulation in PeRo-Lum1 cells, the basal expression level of these genes was higher in PeRo-Lum1 cells as compared to PeRo-Bas1 cells, suggesting constitutive activation of ERα signaling. We next determined the top 1,000 overexpressed and the top 1,000 underexpressed genes in the *Pdgfc*$^{-/-}$ cells relative to the *Pdgfc*$^{+/+}$ cells. Compared to 100,000 randomly permuted lists of 1,000 genes, the over- and underexpressed genes were significantly enriched for binding sites of proteins encoded by mouse genes orthologous to human *ESR1*, *FOXA1* and *GATA3* in both MCF7 and T47D cells. (**Fig. 2f–k** and **Supplementary Fig. 6d–g**), indicating activation of a global gene regulatory program signifying luminal tumors in the absence of *Pdgfc*. In further support of the existence of an activated ERα pathway in PeRo-Lum1 cells, gene set enrichment analysis (GSEA) demonstrated that tamoxifen treatment in these cells resulted in enrichment for documented ERα-target genes or genes with documented sensitivity to tamoxifen (**Supplementary Fig. 7**). Additionally, tamoxifen treatment

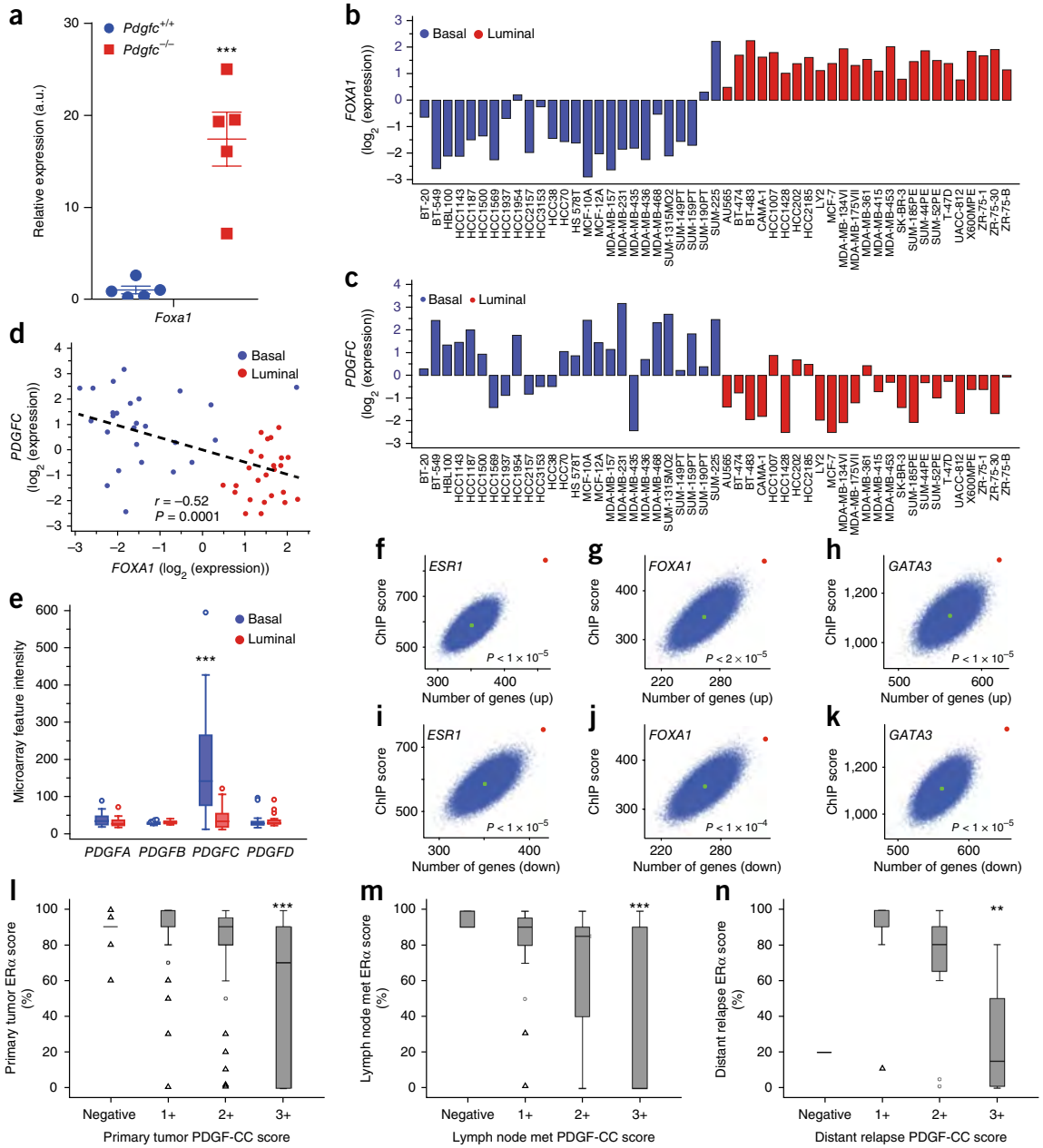

Figure 2 Expression of PDGF-CC in breast carcinomas is associated with the hormone receptor–negative, basal-like molecular subtype. (**a**) Results from qRT-PCR analysis of expression of the luminal subtype marker *Foxa1* in tumors from 14-week-old MMTV-PyMT mice ($n = 5$ mice in each group; analysis performed independently 3 times; mean ± s.e.m. depicted). $^{***}P < 0.001$; two-sided, unpaired, equal variance Student's *t*-test. (**b**,**c**) Expression of *FOXA1* (**b**) and *PDGFC* (**c**) in a panel of 51 breast cancer cell lines[29] divided according to basal-like or luminal-like molecular subtype. (**d**) Correlation between expression of *FOXA1* and *PDGFC* in a panel of 51 breast cancer cell lines divided according to basal-like or luminal-like molecular subtype. Correlation coefficient and *P* value from Pearson correlation analysis of $n = 26$ basal cell lines and $n = 25$ luminal cell lines. (**e**) Expression of all genes in the PDGF family in $n = 26$ basal cell lines and $n = 25$ luminal cell lines. The box represents the interquartile range, the midline represents the average expression and whiskers depict the range of expression with statistical outliers (>2 s.d. from the mean) indicated by circles. $^{***}P = 1 \times 10^{-6}$; two-sided, unpaired Welch's unequal variances *t*-test. (**f**–**k**) Enrichment for binding sites for luminal-defining transcription factors encoded by *ESR1*, *FOXA1*, and *GATA3*, as derived from public data sets from ChIP–seq analyses in MCF7 cells, in the 1,000 most up- and downregulated genes in *Pdgfc*$^{-/-}$ PeRo-Lum1 cells as compared to *Pdgfc*$^{+/+}$ PeRo-Bas1 cells. The red dot represents the query signature of 1,000 up- or downregulated genes; each blue dot represents one out of a total of 100,000 randomly sampled gene lists of equal size to the query signature; the green dot represents the average of the randomly sampled gene lists. The rank of the query gene list divided by the total number of resample instances was then used as a *P* value for the probability to acquire the level of enrichment by chance. (**l**–**n**) Correlation between expression of ERα and PDGF-CC in primary breast carcinomas (**l**: $n = 470$ independent samples; $^{***}P = 2.1 \times 10^{-14}$; two-sided Jonckheere–Terpstra test for ordered alternatives), synchronous lymph node metastases (lymph node met) (**m**: $n = 132$ independent samples; $^{***}P = 1.5 \times 10^{-8}$; two-sided Jonckheere–Terpstra test for ordered alternatives) or asynchronous distant relapses (**n**: $n = 29$ independent samples; $^{**}P = 0.0015$; two-sided Jonckheere–Terpstra test for ordered alternatives) included in the Lund cohort. The box represents the interquartile range, the midline represents the median expression and whiskers depict 1.5× the height of the box. Circles and triangles represent statistical outliers that fall outside of the whiskers and extreme outliers that fall outside of 3× the height of the box, respectively.

Table 2 Spearman's rank correlations of PDGF-CC expression and FOXA1 expression with biomarkers for molecular subtypes in the Zurich Cohort

		FOXA1	ERα	PgR	CK5/6	EGFR
PDGF-CC epithelium	Correlation coefficient	**−0.180**	**−0.485**	**−0.301**	**0.331**	**0.303**
	P value	0.002	0.0001	0.0001	0.0001	0.0002
	n	288	856	854	860	854
FOXA1	Correlation coefficient	1.000	**0.454**	**0.299**	**−0.246**	NA
	P value	NA	0.0001	0.0001	0.0001	NA
	n	315	285	309	310	NA

Correlation coefficients in bold are statistically significant.

of *Pdgfc*$^{-/-}$ breast cancer cells induced expression of a gene profile related to decreased cell cycle progression, demonstrating manifestation of functional ERα signaling in PeRo-Lum1 cells (**Supplementary Fig. 7**). Finally, we also submitted a list of genes ranked by their correlation to the expression of *PDGFC* in breast tumors included in TCGA to GSEA. In accordance, genes that were inversely related to *PDGFC* expression were part of data sets identifying ERα-target genes, whereas genes that were positively correlated to *PDGFC* expression were part of data sets related to inhibition of ERα signaling (**Supplementary Fig. 8**). Jointly, our analyses, which used a diverse set of approaches, strongly point to an association between the absence of expression of *PDGFC* and a luminal phenotype characterized by functional ERα signaling.

Next, we further investigated the association of PDGF-CC expression with the molecular subtype of breast cancer through analysis of expression of basal-like and luminal markers in the Zurich cohort of human breast tumors using immunostaining (**Table 2** and **Supplementary Fig. 9**). Strikingly, PDGF-CC showed a strong correlation with the basal-like markers cytokeratin (CK) 5/6 and epidermal growth factor receptor (EGFR), whereas low expression of PDGF-CC was associated with hormone receptor-positive tumors expressing FOXA1, ERα and PgR (**Table 2**). The inverse correlation between PDGF-CC and hormone receptors was further corroborated in the Lund cohort, in which the relationship was also established in synchronous lymph node metastases and asynchronous distant metastases (**Fig. 2l–n** and **Supplementary Table 5**). Only 7.8% of tumors of the luminal A subgroup of breast cancers were positive for PDGF-CC in the primary tumor epithelium, whereas 71.9% of triple-negative tumors were positive (**Supplementary Table 6**). Taken together, we have revealed a close association between expression of PDGF-CC and hormone receptor–negative breast tumors in cohorts of human patients.

A paracrine signaling circuit in stromal fibroblasts established by PDGF-CC determines the molecular subtype of breast tumor cells

We next investigated the molecular mechanisms through which paracrine signaling by epithelium-derived PDGF-CC was associated with basal-like features of breast tumors. Culture in medium conditioned with the immortalized breast CAF cell line CAF2 (ref. 31) significantly reduced the sensitivity of PeRo-Lum1 mammary carcinoma cells with luminal features isolated from a tumor in a MMTV-PyMT; *Pdgfc*$^{-/-}$ mouse to tamoxifen-induced growth arrest (**Fig. 3a**). This finding suggests that secreted factors from stromal fibroblasts confer resistance to endocrine therapy. Next, we stimulated CAF2 cells with PDGF-CC and performed global transcriptional analysis. A list of statistically significantly upregulated genes (fold change > 1.4) was generated and filtered for gene ontology terms 'Extracellular space' and 'Extracellular region'. The resulting list of genes was used to generate hypotheses concerning which factors mediated the effect of PDGF-CC, and candidate secreted proteins, for which expression was highly induced by PDGF-CC, were tested for their ability to regulate the sensitivity of luminal breast cancer cells to the action of tamoxifen. The most significantly upregulated genes, namely stanniocalcin 1 (*Stc1*), hepatocyte growth factor (*Hgf*) and insulin growth factor binding protein 3 (*Igfbp3*), were validated using qRT-PCR to ensure robust induction by PDGF-CC in CAF2 cells after 48 h of stimulation (**Supplementary Fig. 10**). Strikingly, pretreatment with a cocktail of the CAF-derived factors HGF, IGFBP3 and STC1 reduced the sensitivity of PeRo-Lum1 cells to tamoxifen-induced growth arrest (**Fig. 3b**). We also assessed whether stimulation of PeRo-Lum1 cells with HGF, IGFBP3 and STC1 converted their ERα-positive phenotype into an ERα-negative phenotype. Indeed, although each factor alone affected the expression of luminal markers encoded by *Esr1*, *Foxa1* and *Gata3* to some degree, the concerted action of HGF, IGFBP3 and STC1 substantially suppressed the luminal-like features of *Pdgfc*$^{-/-}$ mammary carcinoma cells (**Fig. 3c–e**). The expression of HGF, IGFBP3 and STC1 by CAFs populating the stroma of tumors from MMTV-PyMT; *Pdgfc*$^{+/+}$ mice was further confirmed through immunostaining (**Fig. 3f–h**). Reassuringly, in breast tumors from the TCGA cohort, the levels of expression of *PDGFC*, *HGF* and *IGFBP3* were all significantly, albeit modestly, correlated to each other and to that of *FOXC1*, which encodes a transcriptional regulator associated with the basal-like phenotype[32] (**Fig. 3i**), suggesting there is also commonality in their regulation in human tumors. By contrast, and in line with our observations, the expression of *PDGFC*, *HGF* and *IGFBP3* were inversely correlated with expression of the luminal marker–encoding genes *FOXA1*, *ESR1* and *GATA3* (**Fig. 3i**). In support of this result, a cohort of 43 triple-negative breast cancer specimens displayed a close correlation between the expression of HGF, IGFBP3 and STC1 in the tumor stroma (**Supplementary Fig. 11a–c** and **Supplementary Table 7**). All three factors were also variably expressed by the tumor epithelium, but a lack of close correlation in expression indicates distinct mechanisms of gene regulation (data not shown). Similarly, immunostaining and scoring of a representative selection of 58 human breast tumors included in the Tam2Y cohort[33] for epithelial PDGF-CC, stromal HGF, stromal IGFBP3 and stromal STC1 demonstrated a close correlation of the expression of each of these markers with one another and with a basal-like, ERα-negative phenotype (**Supplementary Table 8**). In summary, paracrine signaling through PDGF-CC stimulates the expression of HGF, IGFBP3 and STC1 in breast CAFs from luminal tumors, leading to a malignant cell phenotype denoted with lack of ERα and other luminal markers and a reduced sensitivity to tamoxifen.

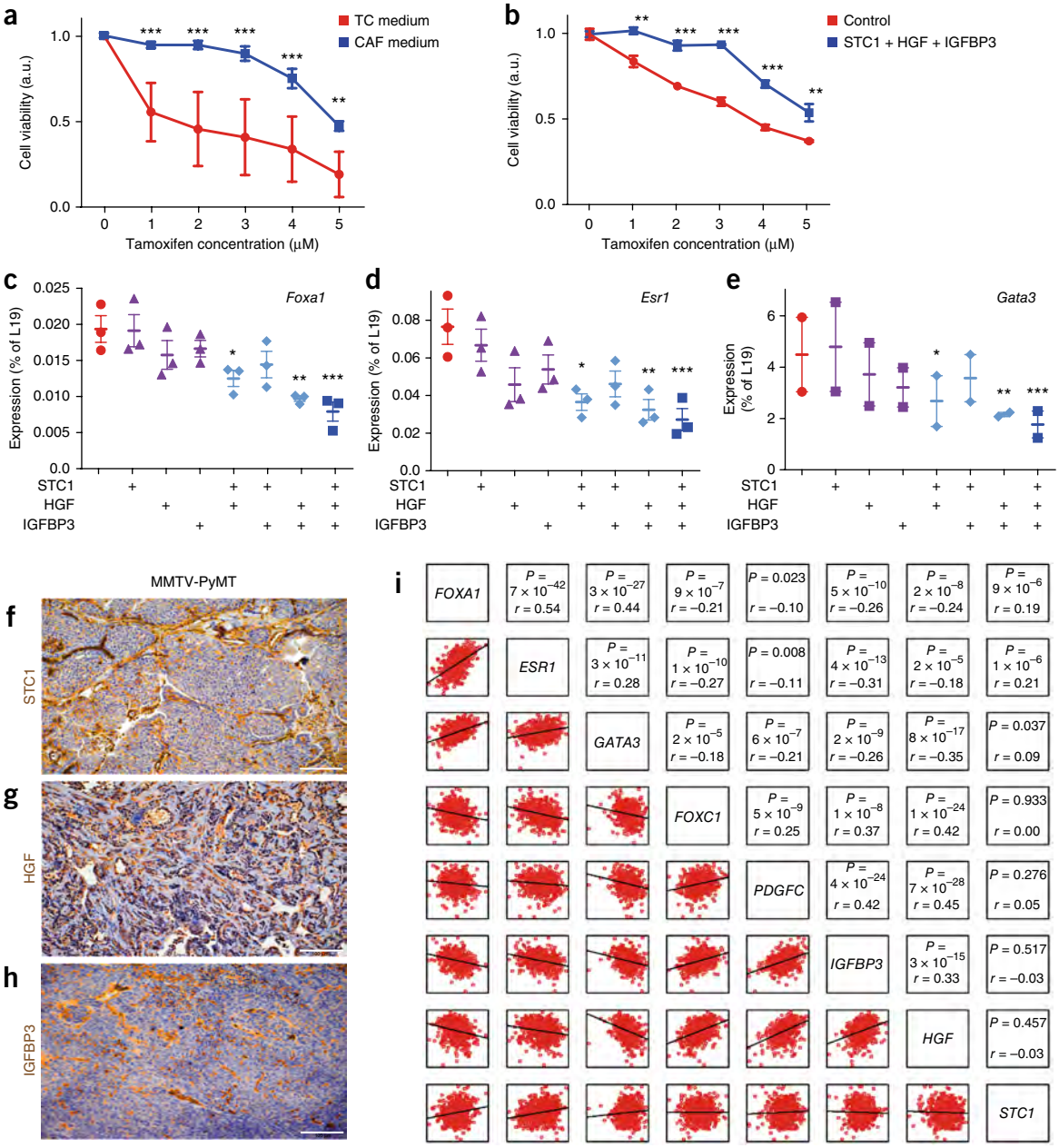

Figure 3 CAF-derived factors whose expression is induced by PDGF-CC reduce the sensitivity of breast tumor cells to endocrine therapy. (**a**) Viability of PeRo-Lum1 luminal breast cancer cells derived from MMTV-PyMT; *Pdgfc*$^{-/-}$ mice in the presence of increasing concentrations of 4-hydroxytamoxifen in medium conditioned by tumor cells (TC) or CAFs (the average (with s.e.m.) of $n = 6$ independent experiments is shown). $^{**}P < 0.01$, $^{***}P < 0.001$; TC medium versus CAF medium at each tamoxifen concentration (1 μM, $P = 0.0001$; 2 μM, $P = 0.00001$; 3 μM, $P = 0.00001$; 4 μM, $P = 0.00001$; 5 μM, $P = 0.005$); two-way ANOVA with P values from Bonferroni *post hoc* correction. (**b**) Viability of PeRo-Lum1 cells in the presence of increasing concentrations of 4-hydroxytamoxifen in medium conditioned by nothing (control) or STC1, HGF and IGFBP3 (the average (with s.e.m.) of $n = 6$ independent experiments is shown). $^{**}P < 0.01$, $^{***}P < 0.001$; control versus STC1 + HGF + IGFBP3 at each tamoxifen concentration (1 μM, $P = 0.003$; 2 μM, $P = 0.0003$; 3 μM, $P = 0.00008$; 4 μM, $P = 0.0002$; 5 μM, $P = 0.005$); two-way ANOVA with P values from Bonferroni *post hoc* correction. (**c**–**e**) Results from qRT-PCR analyses showing the average expression (with s.e.m., depicted as the percentage of expression of the reference gene *L19*) of *Foxa1* (**c**, $n = 3$ independent experiments), *Esr1* (**d**, $n = 3$ independent experiments) or *Gata3* (**e**, $n = 2$ independent experiments) in PeRo-Lum1 cells in the presence of combinations of STC1, HGF and IGFBP3. *Foxa1*: $^{*}P = 0.03$, $^{**}P = 0.002$, $^{***}P = 0.0003$; one-way ANOVA with P values from Bonferroni *post hoc* correction. *Esr1*: $^{*}P = 0.01$, $^{**}P = 0.005$, $^{***}P = 0.001$; one-way ANOVA with P values from Bonferroni *post hoc* correction. *Gata3*: $^{*}P = 0.02$, $^{**}P = 0.007$, $^{***}P = 0.001$; one-way ANOVA with P values from Bonferroni *post hoc* correction. (**f**–**h**) Immunostaining of tissue sections from tumors from 14-week-old MMTV-PyMT mice for STC1 (**f**), HGF (**g**) or IGFBP3 (**h**). Immunostaining was performed $n = 3$ independent times, and representative images from $n = 5$ tumors are shown. Scale bars, 100 μm. (**i**) Pearson's correlation analysis of genes encoding factors denoting luminal-like (*FOXA1*, *ESR1*, *GATA3*) or basal-like (*FOXC1, PDGFC*) molecular subtype. The cross-section of two genes to the left depicts the expression of the two genes in luminal subtype breast carcinomas (each red dot represents one tumor) included in the TCGA cohort (out of $n = 1{,}086$ independent tumors); the black line represents the best fit through the data. The cross-section of two genes to the right states the correlation coefficient and P for the two genes.

Genetic or pharmacological targeting of PDGF-CC sensitizes ERα-negative breast tumors to hormone therapy

ERα expression, which confers sensitivity to endocrine therapy such as tamoxifen, is the most important distinguishing clinical feature of breast tumors of the luminal subtype. We therefore investigated whether targeting PDGF-CC would convey sensitivity to endocrine therapy to previously resistant ERα-negative breast tumors *in vivo*. WT FVB/N mice bearing orthotopically transplanted tumors from MMTV-PyMT; *Pdgfc*$^{+/+}$ or MMTV-PyMT; *Pdgfc*$^{-/-}$ mice were treated daily with tamoxifen starting from the time at which tumors were readily palpable. As expected, due to the lack of ERα expression at this late stage of malignant development, the tumors of tamoxifen-treated MMTV-PyMT; *Pdgfc*$^{+/+}$ mice continued to grow at a rate similar to that of tumors from control-treated mice (**Fig. 4a**). In sharp contrast to the progressive growth of all *Pdgfc*$^{+/+}$ tumors, growth of *Pdgfc*$^{-/-}$ tumors was severely retarded upon treatment with tamoxifen, and 71% (5 of 7) of the treated mice exhibited a complete or partial response (defined as full regression or shrinkage of tumor volume by more than 30%, respectively), in agreement with their expression of ERα (**Fig. 4b**). At the end of the trial, tumors from tamoxifen-treated mice devoid of paracrine PDGF-CC signaling had a volume that was reduced by an average of 17%, whereas control-treated mice presented with tumors that had grown by 624% since treatment initiation, evidently revealing functional sensitization conferred by ERα signaling within *Pdgfc*$^{-/-}$ breast tumors (**Fig. 4b**).

To conclusively demonstrate the utility of agents targeting PDGF-CC for sensitization of breast tumors of the basal-like subtype to the action of tamoxifen, we implanted the triple-negative patient-derived xenografts (PDX) 12.58 and 14.32 as well as the basal-like breast cancer cell line MDA-MB-231 orthotopically into immunocompromised NOD *scid* gamma mice. Indeed, analysis revealed that in 12.58 and MDA-MB-231 tumors, which originally did not express meaningful levels of ERα, expression of ERα was substantially upregulated upon treatment with 6B3, as determined through immunostaining; this result corroborated the role for paracrine signaling through PDGF-CC in establishing a lack of ERα expression in breast tumors of the basal-like subtype (**Fig. 4c–f** and **Supplementary Fig. 12a–d**). The upregulation of ERα expression in 12.58 and MDA-MB-231 tumors following PDGF-CC blockade was not uniform but rather occurred focally in differentiated nests of malignant cells (**Supplementary Fig. 12a–d**). Notably, treatment with 6B3 was sufficient in itself to push 3 of 8 (37.5%) of the basal-like PDX tumors above the threshold, defined as 1% of tumor nuclei in a sample showing ERα positivity, used clinically to mandate treatment with endocrine therapy[34]. As expected, treatment with tamoxifen together with a control antibody was unable to influence the growth of fully established 14.32 or MDA-MB-231 tumors (**Fig. 4g**,**h**). In contrast with this result and in good agreement with conversion to the ERα-positive phenotype seen upon neutralization of PDGF-CC, combined administration of tamoxifen and 6B3 led to significant growth retardation of both 14.32 and MDA-MB-231 tumors (**Fig. 4i**,**j**). The frequency of ERα-positive cancer cells diminished in MDA-MB-231 tumors following tamoxifen therapy in combination with the 6B3 antibody, demonstrating that the induction of ERα expression caused by neutralization of PDGF-CC indeed invoked sensitivity to the action of tamoxifen (**Fig. 4f**). Similarly, pharmacological blockade of PDGF-CC also brought about a delay in growth of MDA-MB-231 xenografts following treatment with the aromatase inhibitor letrozole (**Supplementary Fig. 12e**,**f**), suggesting that the strategy is widely applicable in basal-like tumors for sensitization to endocrine therapies, such as tamoxifen and letrozole, with diverse mechanisms of action. Conversely, mice xenografted with ERα-expressing luminal MCF7 cells with ectopic expression of *Pdgfc* did not respond to tamoxifen therapy in contrast to mice implanted with the parental clone (**Fig. 4k**). Jointly, our studies thus establish functional sensitization of ERα-negative tumors to endocrine therapy as a consequence of conversion to an ERα-positive state through blockade of paracrine signaling by PDGF-CC.

DISCUSSION

We have revealed a paracrine signaling network that manifested in the basal-like breast tumor microenvironment, in which tumor epithelium-derived PDGF-CC orchestrates specification of an ERα-negative phenotype through activation of CAFs that are induced to secrete HGF, IGFBP3 and STC1 (**Fig. 4l**). Blockade of PDGF-CC, either through genetic or pharmacological means, prompted sensitization of previously resistant breast tumors to the action of endocrine therapy through inducing the expression of ERα (**Fig. 4l**). Our findings unexpectedly identify CAFs as functional regulators of the molecular subtype of breast cancer and offer new therapeutic opportunities for a patient group in need of improved treatment options.

The distinguishing features of luminal and basal-like breast cancer cells have been thought to signify different cells of origin, i.e., luminal progenitor cells and breast epithelial stem cells, respectively, in the normal mammary gland[35]. However, recent studies describe a high degree of plasticity and heterogeneity in the definition of luminal or basal-like tumors. Interconversion between luminal and basal-like tumor cells has been demonstrated to occur efficiently *in vitro*, indicating a common progenitor cell origin[36]. Indeed, on the basis of gene expression analysis and functional studies, luminal progenitor cells have been proposed as a common source of luminal and basal-like breast carcinomas[37–40]. Moreover, a phenotypic switch from basal-like to luminal breast cancer can be achieved through expression of *ESR1*, *FOXA1* or *GATA3*, whereas a transition from a basal-like state into a luminal state can result from epigenetic reprogramming[41–43]. Interestingly, cell cultures that were isolated from tumors in *Pdgfc*$^{-/-}$ mice exhibited constitutive ERα signaling and a luminal phenotype while retaining sensitivity to tamoxifen. Such tools may hold important clues as to the nature of the epigenetic programming of the molecular subtype of breast cancer. In line with our work, a recent study demonstrated development of tumors with differential ERα expression in lesions grafted from the same luminal PDX but at different anatomical sites, i.e., the mammary fat pad or the milk ducts, suggesting profound microenvironmental regulation[44]. Rather than searching for new drugs targeting genetic or epigenetic alterations in basal-like breast tumors, pharmacological strategies for the induction of a switch from hormone receptor–negative breast cancer to a luminal subtype would enable use of established and effective treatment options for a large patient group in need of improved therapy. As such, our study, which demonstrates that specification for the luminal or basal-like subtype is under control of the tumor microenvironment through regulation of FOXA1, ERα and GATA3, reveals new opportunities for therapeutic targeting through interference with paracrine signaling between malignant cells and CAFs.

Recent studies have suggested that PDGFR-α expression may be a feature of malignant cells that have properties of stem cells and/or that have undergone the epithelial-to-mesenchymal transition in breast cancer[45,46]. However, we have previously shown that expression of PDGFR-α in malignant cells is not a universal feature of human mammary carcinomas in the Lund cohort, as expression of PDGFR-α in overt cancer cells was only found in 20% of cases[47]. In contrast, virtually

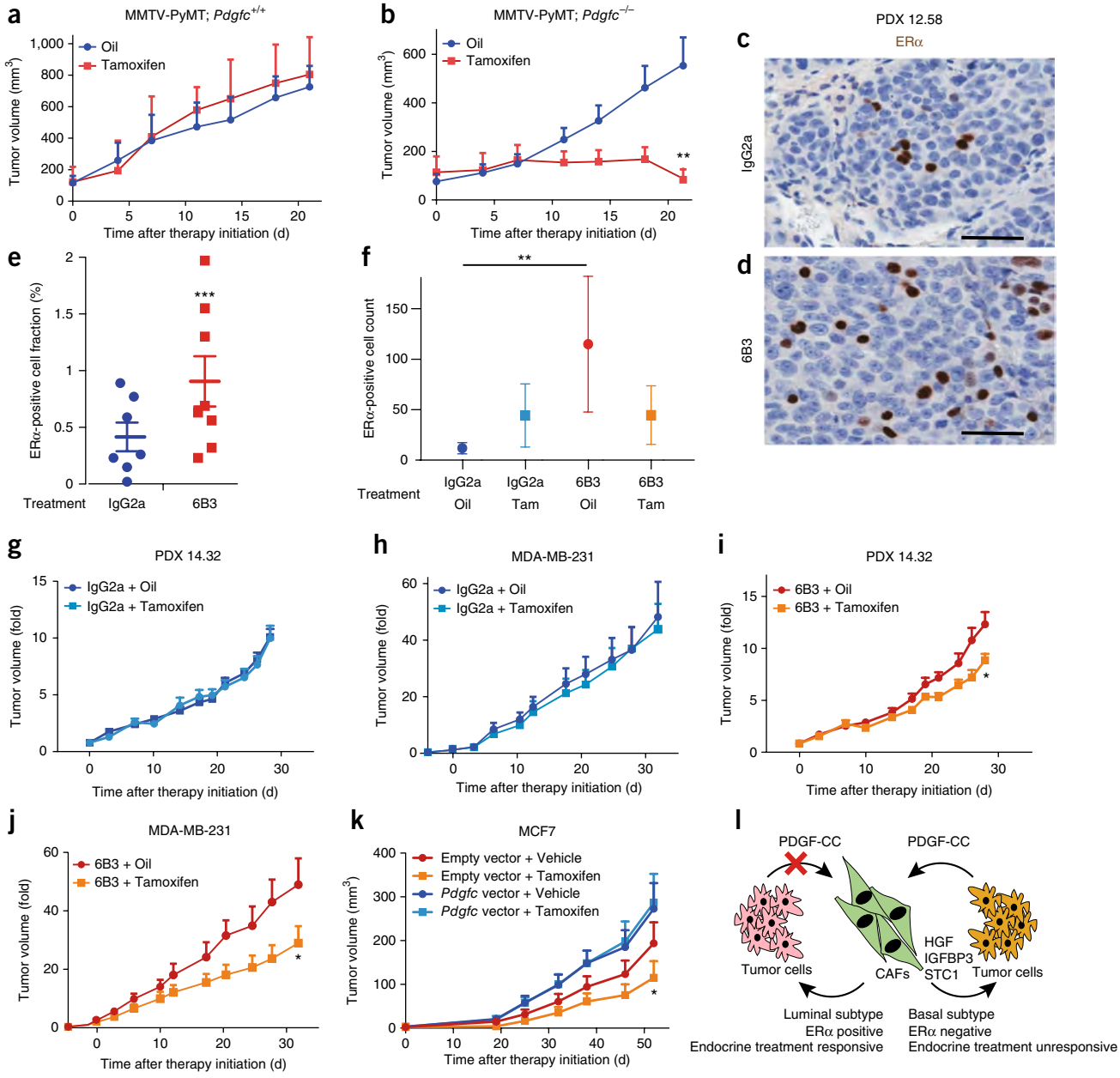

Figure 4 Genetic or pharmacological targeting of PDGF-CC induces expression of ERα and sensitizes tumors to endocrine therapy. (**a**,**b**) Treatment of FVB/n mice transplanted orthotopically with tumors derived from 14-week-old MMTV-PyMT; *Pdgfc*$^{+/+}$ (**a**) or MMTV-PyMT; *Pdgfc*$^{-/-}$ (**b**) mice with oil vehicle ($n = 7$ *Pdgfc*$^{+/+}$ mice and 6 *Pdgfc*$^{-/-}$ mice) or tamoxifen ($n = 6$ *Pdgfc*$^{+/+}$ mice and 7 *Pdgfc*$^{-/-}$ mice). Average tumor volume (with s.e.m.) is depicted. $^{**}P = 0.002$; two-sided, unpaired, equal variance Student's *t*-test. (**c**,**d**) Immunostaining for ERα (brown) of tissue sections from the triple-negative PDX 12.58 from mice treated with control IgG2a or 6B3. Immunostaining was performed $n = 3$ independent times, and representative images are shown. Scale bars, 40 μm. (**e**) Quantification of the average ERα expression (with s.e.m.) in PDX 12.58 from mice treated with control IgG2a or 6B3 ($n = 7$ IgG2a-treated and 8 6B3-treated mice). $^{***}P = 7 \times 10^{-7}$; χ^2 test. (**f**) Quantification of the average number of ERα-expressing cells (with s.e.m.) in MDA-MB-231 tumors from mice treated with control IgG2a or 6B3 in combination with oil vehicle ($n = 10$ IgG2a-treated and 12 6B3-treated mice) or tamoxifen ($n = 12$ IgG2a-treated and 12 6B3-treated mice). $^{**}P = 0.003$; two-sided, unpaired, equal variance Student's *t*-test. (**g**) The average tumor volume (with s.e.m.) in mice carrying orthotopically transplanted triple-negative PDX 14.32 that were treated with control IgG2a in combination with vehicle ($n = 10$ mice) or tamoxifen ($n = 10$ mice). (**h**) The average tumor volume (with s.e.m.) in mice carrying orthotopically transplanted MDA-MB-231 tumors that were treated with control IgG in combination with oil vehicle ($n = 10$ mice) or tamoxifen ($n = 12$ mice). (**i**) The average tumor volume (with s.e.m.) in mice carrying orthotopically transplanted triple-negative PDX 14.32 that were treated with the neutralizing PDGF-CC antibody 6B3 in combination with vehicle ($n = 10$ mice) or tamoxifen ($n = 10$ mice). $^{*}P = 0.03$; two-sided, unpaired, equal variance Student's *t*-test. (**j**) The average tumor volume (with s.e.m.) in mice carrying orthotopically transplanted MDA-MB-231 tumors that were treated with the neutralizing PDGF-CC antibody 6B3 in combination with oil vehicle ($n = 12$ mice) or tamoxifen ($n = 13$ mice). $^{*}P = 0.025$; two-sided, unpaired, equal variance Student's *t*-test. (**k**) The average tumor volume (with s.e.m.) in mice carrying orthotopically transplanted MCF7 tumors that were infected with lentivirus carrying an empty vector or a vector driving *Pdgfc* expression and were treated with oil vehicle (empty vector, $n = 9$ mice; *Pdgfc* vector, $n = 10$ mice) or tamoxifen (empty vector, $n = 10$ mice; *Pdgfc* vector, $n = 8$ mice). $^{*}P = 0.029$; empty vector + tamoxifen versus *Pdgfc* vector + tamoxifen; two-sided, unpaired, equal variance, Student's *t*-test. (**l**) Schematic of the paracrine action of PDGF-CC in the breast tumor microenvironment. An active crosstalk between malignant cells and CAFs that is mediated through PDGF-CC results in specification of the molecular subtype and regulation of sensitivity to endocrine therapy.

all breast tumors in the same cohort harbored CAFs expressing PDGFR-α and PDGFR-β, strongly indicating that the paracrine mode of signaling through PDGF-CC and not autocrine signaling is the most prominent route of signal transduction in human breast cancers. Stimulation of breast CAFs with PDGF-CC induced the expression of HGF, IGFBP3 and STC1. Previous studies using conditional gene targeting of *Pdgfra* have demonstrated a reduced expression of HGF and collagen by fibroblasts compared to genetically normal fibroblasts, lending support to our findings[48]. Expression of MET, the receptor for HGF, has also been associated with basal-like breast cancer, in agreement with results from our study[49–52]. Intriguingly, constitutive activation of MET signaling drives commitment of luminal progenitor cells to a basal-like cell fate[53]. In the case of IGFBP3, the association with hormone receptor–negative breast cancers and poor survival is already well established, although a causal relationship has not been reported previously[54].

Mesenchymal cells are highly plastic entities. Normal fibroblasts are described as counteracting tumorigenesis through repressing cancer initiation[14,55,56]. However, coevolution of the malignant epithelium and its underlying stroma instigates activation of CAFs into a phenotype supporting most, if not all, hallmarks of cancer progression[11,57]. Abundant evidence thus supports the utility of CAFs as drug targets by virtue of their tumor-promoting abilities. Indeed, a recent study identified a subset of CD146-negative CAFs that confer resistance to endocrine therapy in luminal breast cancer[58]. However, investigations of pancreatic adenocarcinoma, a cancer type associated with severe desmoplasia, caution against indiscriminate blockade of CAF recruitment and/or activation[59,60]. Through use of inhibitors of hedgehog signaling or through eradication of α-smooth muscle actin (α-SMA)-expressing CAFs, genetically engineered pancreatic adenocarcinomas were able to thrive in an unrestricted manner. Given the diverse functions described, it is thus likely that CAFs make up a heterogeneous population harboring subsets that either promote or inhibit tumor growth . Nevertheless, despite sometimes aggravating tumorigenesis, blockade of CAF recruitment sensitized pancreatic tumors to anti-angiogenic therapy and to immune-checkpoint inhibitors[59,60]. Similarly, we found that blockade of signaling through PDGF-CC was useful as a combination partner to endocrine therapy in experimental mammary carcinomas. Therapeutic targeting of CAFs may thus best be exploited in joint treatment regimens with drugs impinging on multiple cell types and signaling pathways that collectively sustain malignant growth.

The work presented here identifies a hitherto unappreciated role for the tumor microenvironment in the specification of the molecular subtype of breast cancer and distinguishes PDGFR-α-expressing CAFs as a promising pharmacological target to achieve manifestation of ERα in mammary carcinomas. As such, our discovery of neutralization of PDGF-CC as an efficacious combination partner to endocrine therapy justifies clinical evaluation for the treatment of patients with basal-like breast cancer.

METHODS

Methods, including statements of data availability and any associated accession codes and references, are available in the online version of the paper.

Note: Any Supplementary Information and Source Data files are available in the online version of the paper.

ACKNOWLEDGMENTS

We gratefully acknowledge expert help with pathology assessments from the late D. Grabau and provision of the Tam2Y cohort by M. Fernö. Further, we would like to thank D. Cao, M. O'Brien and C. Murone for their technical support and P.-O. Bendahl for statistical assistance. K.P. is the Göran & Birgitta Grosskopf Professor at Lund University. The research presented herein was supported by grants from the following agencies to K.P.: a Consolidator Grant from the European Research Council (the TUMORGAN project, grant 309322), the Swedish Research Council, the Swedish Cancer Society, the STARGET consortium (a Swedish Research Council Linnaeus network), BioCARE and Lund University. U.E. acknowledges funding support from the Swedish Research Council, the Swedish Cancer Society, Karolinska Institutet and Ludwig Institute for Cancer Research. A.M.S. acknowledges funding support from National Health and Medical Research Council (NHMRC) Fellowship 1084178 and Grant 10927888 and the Operational Infrastructure Support Program provided by the Victorian Government, Australia.

AUTHOR CONTRIBUTIONS

P.R. generated and analyzed data and conceived the study. M. Bocci, M. Bartoschek, H.L., G.K., S.J., S.L., J.S., C.L., P.E., S.R., C.A., E. Cortez, L.H.S., C.O.-P., B.K.H. and J.H. generated and analyzed data. E. Cordero, I.J.G.B. and E.L. generated data. A.O. provided exclusive reagents. M.H. analyzed data. L.R., H.M. and A.M.S. analyzed data and provided exclusive reagents. U.E. analyzed data, provided exclusive reagents and conceived the study. K.P. generated and analyzed data, conceived the study, managed the study and wrote the manuscript.

COMPETING INTERESTS

K.P., U.E. and P.R. are named inventors on Patent Cooperation Treaty (PCT) application no. PCT/EP2016/077295, which is related to the findings of the current study. K.P., U.E. and A.M.S. are shareholders of Paracrine Therapeutics, which develops inhibitory agents to PDGF-CC.

1. Perou, C.M. *et al.* Molecular portraits of human breast tumours. *Nature* **406**, 747–752 (2000).
2. Goldhirsch, A. *et al.* Thresholds for therapies: highlights of the St Gallen International Expert Consensus on the primary therapy of early breast cancer 2009. *Ann. Oncol.* **20**, 1319–1329 (2009).
3. Sørlie, T. *et al.* Gene expression patterns of breast carcinomas distinguish tumor subclasses with clinical implications. *Proc. Natl. Acad. Sci. USA* **98**, 10869–10874 (2001).
4. Goldhirsch, A. *et al.* Personalizing the treatment of women with early breast cancer: highlights of the St Gallen International Expert Consensus on the Primary Therapy of Early Breast Cancer 2013. *Ann. Oncol.* **24**, 2206–2223 (2013).
5. Goldhirsch, A. *et al.* Strategies for subtypes—dealing with the diversity of breast cancer: highlights of the St. Gallen International Expert Consensus on the Primary Therapy of Early Breast Cancer 2011. *Ann. Oncol.* **22**, 1736–1747 (2011).
6. Prat, A. *et al.* Clinical implications of the intrinsic molecular subtypes of breast cancer. *Breast* **24** (Suppl. 2), S26–S35 (2015).
7. Ignatiadis, M. & Sotiriou, C. Luminal breast cancer: from biology to treatment. *Nat. Rev. Clin. Oncol.* **10**, 494–506 (2013).
8. Voduc, K.D. *et al.* Breast cancer subtypes and the risk of local and regional relapse. *J. Clin. Oncol.* **28**, 1684–1691 (2010).
9. Prat, A. & Perou, C.M. Deconstructing the molecular portraits of breast cancer. *Mol. Oncol.* **5**, 5–23 (2011).
10. Hanahan, D. & Coussens, L.M. Accessories to the crime: functions of cells recruited to the tumor microenvironment. *Cancer Cell* **21**, 309–322 (2012).
11. Pietras, K. & Ostman, A. Hallmarks of cancer: interactions with the tumor stroma. *Exp. Cell Res.* **316**, 1324–1331 (2010).
12. Kalluri, R. & Zeisberg, M. Fibroblasts in cancer. *Nat. Rev. Cancer* **6**, 392–401 (2006).
13. Cortez, E., Roswall, P. & Pietras, K. Functional subsets of mesenchymal cell types in the tumor microenvironment. *Semin. Cancer Biol.* **25**, 3–9 (2014).
14. Augsten, M. Cancer-associated fibroblasts as another polarized cell type of the tumor microenvironment. *Front. Oncol.* **4**, 62 (2014).
15. Kim, H.M., Jung, W.H. & Koo, J.S. Expression of cancer-associated fibroblast related proteins in metastatic breast cancer: an immunohistochemical analysis. *J. Transl. Med.* **13**, 222 (2015).
16. Anderberg, C. *et al.* Paracrine signaling by platelet-derived growth factor-CC promotes tumor growth by recruitment of cancer-associated fibroblasts. *Cancer Res.* **69**, 369–378 (2009).
17. Pietras, K., Pahler, J., Bergers, G. & Hanahan, D. Functions of paracrine PDGF signaling in the proangiogenic tumor stroma revealed by pharmacological targeting. *PLoS Med.* **5**, e19 (2008).
18. Li, X. *et al.* PDGF-C is a new protease-activated ligand for the PDGF α-receptor. *Nat. Cell Biol.* **2**, 302–309 (2000).
19. Cao, R. *et al.* Angiogenesis stimulated by PDGF-CC, a novel member in the PDGF family, involves activation of PDGFR-αα and -αβ receptors. *FASEB J.* **16**, 1575–1583 (2002).

20. Theurillat, J.P. *et al.* NY-ESO-1 protein expression in primary breast carcinoma and metastases: correlation with CD8+ T-cell and CD79a+ plasmacytic/B-cell infiltration. *Int. J. Cancer* **120**, 2411–2417 (2007).
21. Falck, A.K. *et al.* Biomarker expression and St Gallen molecular subtype classification in primary tumours, synchronous lymph node metastases and asynchronous relapses in primary breast cancer patients with 10 years' follow-up. *Breast Cancer Res. Treat.* **140**, 93–104 (2013).
22. Falck, A.K. *et al.* Analysis of and prognostic information from disseminated tumour cells in bone marrow in primary breast cancer: a prospective observational study. *BMC Cancer* **12**, 403 (2012).
23. Guy, C.T., Cardiff, R.D. & Muller, W.J. Induction of mammary tumors by expression of polyomavirus middle T oncogene: a transgenic mouse model for metastatic disease. *Mol. Cell. Biol.* **12**, 954–961 (1992).
24. Lin, E.Y. *et al.* Progression to malignancy in the polyoma middle T oncoprotein mouse breast cancer model provides a reliable model for human diseases. *Am. J. Pathol.* **163**, 2113–2126 (2003).
25. Ding, H. *et al.* A specific requirement for PDGF-C in palate formation and PDGFR-alpha signaling. *Nat. Genet.* **36**, 1111–1116 (2004).
26. Cancer Genome Atlas, N.; Cancer Genome Atlas Network. Comprehensive molecular portraits of human breast tumours. *Nature* **490**, 61–70 (2012).
27. Badve, S. *et al.* FOXA1 expression in breast cancer—correlation with luminal subtype A and survival. *Clin. Cancer Res.* **13**, 4415–4421 (2007).
28. Thorat, M.A. *et al.* Forkhead box A1 expression in breast cancer is associated with luminal subtype and good prognosis. *J. Clin. Pathol.* **61**, 327–332 (2008).
29. Neve, R.M. *et al.* A collection of breast cancer cell lines for the study of functionally distinct cancer subtypes. *Cancer Cell* **10**, 515–527 (2006).
30. Kong, S.L., Li, G., Loh, S.L., Sung, W.K. & Liu, E.T. Cellular reprogramming by the conjoint action of ERα, FOXA1, and GATA3 to a ligand-inducible growth state. *Mol. Syst. Biol.* **7**, 526 (2011).
31. Kojima, Y. *et al.* Autocrine TGF-β and stromal cell-derived factor-1 (SDF-1) signaling drives the evolution of tumor-promoting mammary stromal myofibroblasts. *Proc. Natl. Acad. Sci. USA* **107**, 20009–20014 (2010).
32. Ray, P.S. *et al.* FOXC1 is a potential prognostic biomarker with functional significance in basal-like breast cancer. *Cancer Res.* **70**, 3870–3876 (2010).
33. Chebil, G., Bendahl, P.O., Idvall, I. & Fernö, M. Comparison of immunohistochemical and biochemical assay of steroid receptors in primary breast cancer—clinical associations and reasons for discrepancies. *Acta Oncol.* **42**, 719–725 (2003).
34. Hammond, M.E. *et al.* American Society of Clinical Oncology/College Of American Pathologists guideline recommendations for immunohistochemical testing of estrogen and progesterone receptors in breast cancer. *J. Clin. Oncol.* **28**, 2784–2795 (2010).
35. Polyak, K. Breast cancer: origins and evolution. *J. Clin. Invest.* **117**, 3155–3163 (2007).
36. Gupta, P.B. *et al.* Stochastic state transitions give rise to phenotypic equilibrium in populations of cancer cells. *Cell* **146**, 633–644 (2011).
37. Lim, E. *et al.* Aberrant luminal progenitors as the candidate target population for basal tumor development in BRCA1 mutation carriers. *Nat. Med.* **15**, 907–913 (2009).
38. Molyneux, G. & Smalley, M.J. The cell of origin of BRCA1 mutation-associated breast cancer: a cautionary tale of gene expression profiling. *J. Mammary Gland Biol. Neoplasia* **16**, 51–55 (2011).
39. Liu, S. *et al.* BRCA1 regulates human mammary stem/progenitor cell fate. *Proc. Natl. Acad. Sci. USA* **105**, 1680–1685 (2008).
40. Molyneux, G. *et al.* BRCA1 basal-like breast cancers originate from luminal epithelial progenitors and not from basal stem cells. *Cell Stem Cell* **7**, 403–417 (2010).
41. Su, Y. *et al.* Somatic cell fusions reveal extensive heterogeneity in basal-like breast cancer. *Cell Rep.* **11**, 1549–1563 (2015).
42. Yamamoto, S. *et al.* JARID1B is a luminal lineage-driving oncogene in breast cancer. *Cancer Cell* **25**, 762–777 (2014).
43. Bernardo, G.M. *et al.* FOXA1 represses the molecular phenotype of basal breast cancer cells. *Oncogene* **32**, 554–563 (2013).
44. Sflomos, G. *et al.* A preclinical model for ERα-positive breast cancer points to the epithelial microenvironment as determinant of luminal phenotype and hormone response. *Cancer Cell* **29**, 407–422 (2016).
45. Tam, W.L. *et al.* Protein kinase C α is a central signaling node and therapeutic target for breast cancer stem cells. *Cancer Cell* **24**, 347–364 (2013).
46. Meng, F. *et al.* PDGFRα and β play critical roles in mediating Foxq1-driven breast cancer stemness and chemoresistance. *Cancer Res.* **75**, 584–593 (2015).
47. Jansson, S. *et al.* The three receptor tyrosine kinases c-KIT, VEGFR2 and PDGFRα, closely spaced at 4q12, show increased protein expression in triple-negative breast cancer. *PLoS One* **9**, e102176 (2014).
48. Horikawa, S. *et al.* PDGFRα plays a crucial role in connective tissue remodeling. *Sci. Rep.* **5**, 17948 (2015).
49. Kim, Y.J. *et al.* MET is a potential target for use in combination therapy with EGFR inhibition in triple-negative/basal-like breast cancer. *Int. J. Cancer* **134**, 2424–2436 (2014).
50. Ho-Yen, C.M. *et al.* C-Met in invasive breast cancer: is there a relationship with the basal-like subtype? *Cancer* **120**, 163–171 (2014).
51. Ponzo, M.G. *et al.* Met induces mammary tumors with diverse histologies and is associated with poor outcome and human basal breast cancer. *Proc. Natl. Acad. Sci. USA* **106**, 12903–12908 (2009).
52. Graveel, C.R. *et al.* Met induces diverse mammary carcinomas in mice and is associated with human basal breast cancer. *Proc. Natl. Acad. Sci. USA* **106**, 12909–12914 (2009).
53. Gastaldi, S. *et al.* Met signaling regulates growth, repopulating potential and basal cell-fate commitment of mammary luminal progenitors: implications for basal-like breast cancer. *Oncogene* **32**, 1428–1440 (2013).
54. Marzec, K.A., Baxter, R.C. & Martin, J.L. Targeting insulin-like growth factor binding protein-3 signaling in triple-negative breast cancer. *BioMed Res. Int.* **2015**, 638526 (2015).
55. Bissell, M.J. & Hines, W.C. Why don't we get more cancer? A proposed role of the microenvironment in restraining cancer progression. *Nat. Med.* **17**, 320–329 (2011).
56. Marsh, T., Pietras, K. & McAllister, S.S. Fibroblasts as architects of cancer pathogenesis. *Biochim. Biophys. Acta* **1832**, 1070–1078 (2013).
57. Gascard, P. & Tlsty, T.D. Carcinoma-associated fibroblasts: orchestrating the composition of malignancy. *Genes Dev.* **30**, 1002–1019 (2016).
58. Brechbuhl, H.M. *et al.* Fibroblast subtypes regulate responsiveness of luminal breast cancer to estrogen. *Clin. Cancer Res.* **23**, 1710–1721 (2017).
59. Özdemir, B.C. *et al.* Depletion of carcinoma-associated fibroblasts and fibrosis induces immunosuppression and accelerates pancreas cancer with reduced survival. *Cancer Cell* **25**, 719–734 (2014).
60. Rhim, A.D. *et al.* Stromal elements act to restrain, rather than support, pancreatic ductal adenocarcinoma. *Cancer Cell* **25**, 735–747 (2014).

ONLINE METHODS

Patient cohorts. The Zurich cohort includes tissues from 890 patients with primary invasive breast cancer who were diagnosed at the Institute of Surgical Pathology, University Hospital Zurich between 1965 and 2004 (median, July 1999). All patients enrolled voluntarily under Institutional Review Board–approved protocols, and sample donors gave written informed consent. The medical ethics committee of the Canton Zürichat University Hospital of Zurich approved this study with reference number StV 12-2005. For all of these patients, follow-up data from the cantonal cancer registry were available; patients without follow-up data were not included[20]. Additionally, 69 healthy tissue samples were analyzed. The Lund cohort includes patients with primary breast cancer from a prospective, observational trial evaluating various prognostic markers (the regional ethical review board at Lund University reference numbers, LU692-99 and LU247-01); clinical pathological data and follow-up data have previously been reported[21,23]. Written informed consent was obtained from all patients. Breast cancer–specific mortality was used as the endpoint, and data on survival was retrieved from the Swedish Register of Causes of Death (Central Statistics Office). All events until December 2010 were recorded. The specimens from the Tam2Y cohort were mainly obtained from postmenopausal patients with stage 2 breast carcinoma from the South Swedish Health Care Region between 1985 and 1994 (ref. 33). For the current study, a representative subset of 58 tumors from the cohort was analyzed. The cohort of human triple-negative breast cancers was obtained commercially (Abcam, ab214756) and consisted of 43 evaluable specimens.

Immunohistochemistry analysis of human tumor tissue arrays. To assess PDGF-CC expression in clinical samples, the monoclonal PDGF-CC antibody 6B3 (2 µg/ml) was used on an automated Ventana platform (protocol CC1m for pretreatment, UView HRP detection system). Specific immunoreactivity was fully blocked by an excess of active PDGF-CC. The basal cell marker cytokeratin CK5/6 (1:25, clone cocktail D5/16B4, Dako), HER2 (1:50, clone 10A7 Novocastra, UK), EGFR (prediluted, clone 3C6, Ventana) and Ki-67 (1:20, clone Mib-1, Dako) were processed in parallel. Additionally, immunostaining was performed for HGF (1:100, Abcam ab83760), IGFBP3 (1:100, Santa Cruz Biotechnology sc-9028) and STC1 (1:100, Santa Cruz Biotechnology sc-30183).

Mice. All mouse experiments were approved by the local Ethical Committees for Animal Experimentation in Stockholm North, application N96/11, and in Lund, application M142/13 or by the Austin Health Animal Ethics Committee. Experiments were conducted in compliance with the Australian Code for the care and use of animals for scientific purposes. FVB/N-Tg(MMTV-PyVT)634Mul/J transgenic mice have been described previously[23] and were purchased from The Jackson Laboratory. The presence of the MMTV-PyMT transgene and the heterozygous or homozygous knockout of the *Pdgfc* allele[25] in mice were verified through genotyping. DNA was prepared from either ear or tail biopsies following a common protocol for tissue lysis, nucleic acid extraction and purification. The primer pairs used were as follows: MMTV-PyMT: F, 5′-GGAAGCAAGTACTTCACAAGGG-3′ and R, 5′-GGAAAGTCACTAGGAGCAGGG-3′; WT *Pdgfc*: F, 5′-AGCTGACAT TTGATGAGAGAT-3′ and R, 5′-AGTAGGTGAAATAAGAGGTGAACA-3′; mutated *Pdgfc*: F, 5′-CTCATGTTCTCGTGACTCTGA-3′ and R, 5′-TAGCTAGTCGATACCGTCGA-3′.

Mice deficient for *Pdgfc* were originally on the C57Bl/6 background and backcrossed to the FVB/N background for ten generations before analysis was commenced. Female mice were used in the studies. In all cases, WT littermate mice were used as controls for the genetically engineered mice.

Mouse experiments. The size of the tumor in each of the ten mammary glands in transgenic MMTV-PyMT mice was measured at 12 weeks of age using a caliper. Tumor volume was calculated as length × width^2 × (π / 6). The endpoint for survival analysis was taken as the time at which the combined tumor burden surpassed the ethical guidelines in our permit.

For transplantation experiments, FVB/N female mice aged 3 weeks were anesthetized and maintained under isoflurane during the surgical procedure. A 4-mm incision under the nipple of the right abdominal mammary gland created a pocket where a tumor piece (pieces were derived from either MMTV-PyMT; *Pdgfc*$^{+/+}$ mice or MMTV-PyMT; *Pdgfc*$^{-/-}$ mice and were kept on ice) that was 2 × 2 mm was inserted. Suturing was performed with 6-0 Ethilon polyamide filament (Ethicon). Carpofen (Rimadyl; 5 mg per kg body weight; Orion Pharma Animal Health), a pain-killer and an anti-inflammatory drug, was injected intraperitoneally at the end of the surgical procedure and for the following 2 d. Tumor growth was monitored and measured in sedated mice twice per week with a caliper.

Mouse mammary cell lines derived from WT or *Pdgfc*$^{-/-}$ MMTV-PyMT mice established in our laboratory were orthotopically injected into the fourth inguinal mammary gland of WT FVB/N mice. Tumor growth was monitored and measured in sedated mice twice per week with a caliper.

For therapeutic studies, 2 × 10^6 human MDA-MB-231 cells were inoculated orthotopically in *scid* mice. Prior to tumor inoculation, mice were randomly assigned to receive treatment with anti-PDGF-C (mouse monoclonal antibody clone 6B3) antibody or IgG2a isotype control antibody (Bio X Cell), which was delivered via intraperitoneal injection twice per week (300 µg per week) starting from the day of tumor establishment. For therapeutic trials involving endocrine therapy, when a tumor was palpable (longest diameter >3 mm), mice were alternately assigned into the treatment groups, in which mice were treated with tamoxifen (1 mg per dose via oral gavage daily, Sigma) that was dissolved in a vehicle of ethanol and corn oil (Sigma) through heating the mixture to 55 °C or with vehicle alone. All therapeutic administrations were open label.

For all transplantation experiments, tumor growth was monitored and measured in sedated mice twice per week using a caliper.

Patient-derived xenografts. A total of eight mice (NOD *scid* gamma, NSG) were implanted with tumor pieces that were 1–2 mm^3 in size and were derived from patients with triple-negative breast cancers with documented high expression of PDGF-CC (12.58: *BRCA2* mutation, derived from liver metastasis, treatment resistant; 14.32: derived from primary tumor, treatment naive). Two tumor pieces were implanted per mouse in two mammary fat pads, one on each side of the mouse. Ten days after implantation, mice received anti-PDGF-CC therapy (50 mg ch6B3 per kg body weight, three times per week) or vehicle control (PBS). Tumors were harvested and fixed in 10% formalin. 4-µm sections of the paraffin-embedded tumors were mounted onto SuperFrost Plus slides (Menzel-Glaser, Braunschweig, Germany), deparaffinized and rehydrated before antigen retrieval for 36 min at 95 °C in cell conditioning 1 (CC1) buffer (Ventana Medical Systems Inc., Tuscon, AZ, USA). Ready-to-use CONFIRM anti-ER antibody, clone SP1 (Ventana Medical Systems Inc.) was applied to sections for 40 min at 36 °C. To allow visualization of the immunostaining, sections were incubated with the UltraView Universal DAB Detection Kit (Ventana Medical Systems Inc.) and counterstained with Mayer's haematoxylin. The staining was performed using the Ventana BenchMark Ultra automated immunohistochemical staining instrument (Ventana Medical Systems Inc.).

Mouse tissue preparation, histology and immunostaining. To preserve tissues for downstream analysis, mice were heart-perfused with PBS followed by 4% paraformaldehyde. For paraffin-embedding, organs were postfixed in 4% paraformaldehyde for 12 h at 4 °C. Paraffin-embedded sections were deparaffinized and rehydrated, which was followed by antigen retrieval in citrate buffer (pH 6; DAKO) in a pressure cooker (for ERα) or in a water bath at 95 °C for 20 min (for STC1, IGFBP3 and HGF). Endogenous peroxidase activity was quenched with 3% H_2O_2 in methanol for 10 min at room temperature, followed by washes with 0.1% BSA in PBS.

ERα staining required subsequent steps using Mouse on Mouse (MOM) blocking reagent (Mouse on Mouse basic kit, Vectorlabs), CAS-block (Life Technologies) and MOM diluent. The primary antibody against estrogen receptor ERα (1:200, clone 1D5; DAKO) was incubated in MOM diluent. CAS-block was used for the blocking and incubation of primary antibodies against STC1 (1:200, sc-30183, Santa Cruz Biotechnology), IGFBP3 (1:200, sc-9028, Santa Cruz Biotechnology) and HGF (1:200, ab83760, Abcam). Primary incubation was performed overnight at 4 °C in a humidified chamber. After washing, the appropriate secondary biotinylated antibodies and the ABC peroxidase system were used (ABC Elite standard kit, Vector Laboratories) with DAB as substrate (Vector Laboratories) to visualize bound primary antibodies.

doi:10.1038/nm.4494

For cryopreservation, the primary tumors and lungs of mice were kept in 30% sucrose at 4 °C overnight, followed by embedding in optimal cutting temperature medium (HistoLab). Frozen sections were fixed in ice-cold acetone, followed by blocking using Serum Free Protein Block (DAKO) for >90 min at room temperature. Primary antibodies directed against PDGFR-α (PE-conjugated, 1:200, 12-1401 eBioscience) and PDGFR-α (1:200, 3169S, Cell Signaling) were incubated overnight at 4 °C in a humidified chamber. The appropriate AlexaFluor488-conjugated secondary antibody (Life Technologies) was used to visualize bound primary antibody, and sections were mounted using DAPI-containing mounting media (Vector Laboratories).

Imaging was performed using an upright microscope (Eclipse E800; Nikon) equipped with Plan Fluor objectives (10×, 0.30 NA; 20×, 0.50 NA; 40×, 0.75 NA; Nikon) at room temperature in air. Images were acquired using a SPOT RTKE camera using the SPOT advanced software (Diagnostic Instruments, Inc.).

β-galactosidase staining. Fresh frozen sections were left to dry at room temperature for 15 min before washing in permeabilization solution (4mM $MgCl_2$, 0.04% NP-40, 0.02% deoxycholic acid sodium salt in PBS) 2 × 30 min. Sections were further subjected to X-Gal solution (5mM $K_3Fe(CN)_6$, 5mM $K_4Fe(CN)_6$, 1 mg/ml 5-bromo-4-chloro-3-indole-6-D-galactosidase) and incubated overnight at 37 °C in a humidified chamber. After washing in permeabilization solution 3 × 30 min, sections were counterstained with Nuclear Fast Red solution (Sigma), dehydrated and mounted in Pertex (Histolab).

Assessment of tumor grade. Tumor tissue from MMTV-PyMT; *Pdgfc*$^{+/+}$, MMTV-PyMT; *Pdgfc*$^{+/-}$ and MMTV-PyMT; *Pdgfc*$^{-/-}$ mice (n = 5 mice per genotype, 10 tissue sections per mouse) was classified into different degrees of progression through quantification of the area of transformed glands occupied by tumors at each of the following stages: progression moves from normal fat tissue to a 'precancerous stage' characterized by premalignant hyperplasia and adenoma (with the retention of some normal ductal and acinar mammary gland morphology) to a more epithelial cell–dense 'early carcinoma' with stromal invasion and finally to an invasive, very dense, high-mitotic-index 'late-stage carcinoma'. Tumors were evaluated for the proportion of mammary fat tissue, hyperplastic tissue, adenoma, early carcinoma and late carcinoma. Necrosis was determined by a pathologist and scored blindly in the samples.

Quantification of metastases. The lungs of MMTV-PyMT mice were embedded in paraffin upon tissue fixation. The metastatic burden was assessed through serial sectioning of the entire lung. Following H&E staining of every 25th section, the number of metastatic foci (>8 cells in diameter) was determined in at least 15 tissue sections per lung.

qRT-PCR. For RNA isolation and preparation, primary tumors were snap-frozen and stored at −80 °C; cell cultures were scraped in PBS with a rubber policeman and centrifuged for 2 min at 180*g* so they formed a pellet. RNA was isolated using RNeasy Mini Kit (Qiagen). cDNA was prepared using iScript cDNA Synthesis Kit (Bio Rad). KAPA SYBR FAST qPCR Kit Master Mix (KAPA Biosystems) was used for qPCR. mRNA expression was normalized to that of the housekeeping gene *L19*. For *Foxa1*, *Esr1*, *Pdgfra*, *Fsp1*, and *Acta2*, QuantiTect Primer assays (Qiagen) were used. The following primer pairs were used: *L19*: F, 5′- GGTGACCTGGATGAGAAGGA-3′ and R, 5′-TTCAGCTTGTGGATGTGCTC; *Gata3*: F, 5′- CAATGCCTGCGGACTCTACC-3′ and R, 5′-GGTGGTGGTCTCGACAGTTCG-3′.

qRT-PCR array. RNA isolation and cDNA synthesis was performed as described above. A qPCR array analyzing 84 mammary cancer–specific genes was run according to the manufacturer's instructions (Mouse Breast cancer RT^2 Profiler PCR array, Qiagen). In brief, cDNA was mixed with 2× RT^2 SYBR Green ROX FAST Mastermix and diluted with RNase-free H_2O and added to the RT^2 Profiler PCR Array. The PCR was run for 40 cycles of: (1) 95 °C for 15 s, (2) 60 °C for 30 s, and (3) 72 °C for 30 s. Five tumors derived from MMTV-PyMT; *Pdgfc*$^{+/+}$ mice and five tumors derived from MMTV-PyMT; *Pdgfc*$^{-/-}$ mice transplanted into FVB/n mice were run in the qRT-PCR array.

Western blot. A piece of tumor was minced in liquid N_2 before homogenization in lysis buffer (50 mM Tris-HCl, pH 7.4, 150 mM NaCl, 5 mM EDTA, 1% Triton-X 100, 1% SDS with the addition of Roche Complete protease inhibitor and PhosSTOP) using a Precellys 24 instrument (Bertin Technologies). After 30 min of incubation at 4 °C followed by centrifugation for 10 min at 16,000*g*, the supernatant was collected and further subjected to sonication using Vibra-cell (Sonics & Materials, Inc.). The lysate was centrifuged at 16,000*g*, and the pellet was discarded. Protein concentration was determined using the Pierce BCA Protein Assay Kit, and measurement of the absorption was performed at 562 nm on a spectrophotometer. The protein suspension was mixed with 5× NuPAGE LDS Sample Buffer and NuPAGE Sample Reducing Agent (Life Technologies), denaturated at 96 °C for 10 min and separated by SDS-PAGE on a NuPAGE 4–12% polyacrylamide gel (Life Technologies). The proteins were transferred to a nitrocellulose filter using a dry blotting system (iBlot 2, Life Technologies). The membrane was blocked for 1 h with 5% BSA in TBST (0.1% Tween-20 in TBS) and incubated at 4 °C with primary antibodies (anti-FOXA1, 1:200, sc-6553, Santa Cruz Biotechnology Inc.; anti-ERα, 1:200, sc-542 Santa Cruz Biotechnology Inc.; anti-β-actin 1:5,000, ab-8227 Abcam) in 5% BSA in TBST. After washing, secondary antibodies (rabbit anti–goat IgG (Invitrogen, A27014; goat anti-rabbit IgG (Invitrogen, A27036)) were applied in 5% BSA in TBST and incubated for 1 h at room temperature. The membrane was washed and developed with Amersham ECL Prime Western Blotting Detection Reagent (GE Healthcare Life Sciences). Luminescence signal was measured using FluorChem Q imaging system (Alpha Innotech).

Cell culture. All cells were tested and found to be negative for mycoplasma infection routinely. PeRo-Bas1 cells and PeRo-Lum1 cells were derived from tumors in 12-week-old MMTV-PyMT; *Pdgfc*$^{+/+}$ mouse and MMTV-PyMT; *Pdgfc*$^{-/-}$ mouse, respectively. Human MDA-MB-231 and MCF7 cells were obtained from the American Tissue Type Collection. CAF2 is an immortalized cell line of human fibroblasts conditioned by tumor cells *in vivo* in mice[31]. All cells were maintained in culture in DMEM Glutamax (Invitrogen) that was supplemented with 1% penicillin–streptomycin and 10% FBS.

Gene expression analyses of human breast tumors and cell lines. RNA-seq data from 1,086 breast tumors included in TCGA were analyzed for gene expression and correlation to molecular subtype (http://cancergenome.nih.gov/, downloaded January 30, 2015). Using R (v3.1.1), the data were $\log_2$ transformed, and breast cancer subtypes were classified using the PAM50 centroids[61] after centering the data around the median. For analysis of gene expression in breast cancer cell lines, data for 51 breast cancer cell lines was obtained from ref. 29. Probe-level data were merged on Entrez Gene IDs, centered, $\log_2$ transformed and plotted using MedCalc v11 (MedCalc Software, Belgium). For transcriptional analysis of genes with expression induced by the stimulation of PDGF-CC in CAFs, starved CAF2 cells were stimulated for 48 h with 100 ng/ml of PDGF-CC. Next, RNA was extracted as described above, and samples with RNA integrity number > 9 were subjected to cDNA library preparation and RNA-seq.

***In vitro* cell culture assays.** Candidate proteins for mediating the effect of PDGF-CC on the molecular subtype of breast cancer cells were selected from a list of genes predicted to encode secreted proteins (Gene Ontology terms: 'Extracellular space' and 'Extracellular region') and were found to be upregulated in CAF2 cells following stimulation with PDGF-CC.

3×10^6 PR-Lum1 cells were seeded in culture medium. After 24 h, the cells were starved for 24 h in DMEM Glutamax (Invitrogen) supplemented with 1% BSA (Sigma Aldrich). The cells were next stimulated with recombinant human STC1 (400 ng/ml; BioVendor), recombinant mouse HGF (30 ng/ml; R&D), recombinant mouse IGFBP3 (250 ng/ml; R&D) or combinations of these factors in starvation medium for 48 h. The cell line CAF2 was used to produce CAF-conditioned medium through incubation for 48 h in starvation medium. For 4-OH-tamoxifen treatment, 15,000 cells were seeded in 96-well plates. After 24 h incubation in growth medium followed by 24 h starvation, the cells were stimulated either with CAF-conditioned medium or recombinant factors, as described before. The cells were treated with increasing concentration of

4-OH-tamoxifen (Sigma Aldrich) in stimulation medium at day 4 and 6 post seeding. The cell proliferation reagent WST-1 (Roche) was used for the viability assay at day 7.

Genomic analysis of breast cancer cell lines. PeRo-Bas1 and PeRo-Lum1 cells were seeded in normal DMEM growth medium for 8 h (10-013-CVR, Corning; supplemented with 10% FBS and 1×PEST) and subsequently starved for 24 h in serum-free DMEM (10-014-CVR, Corning; supplemented with 1% BSA (Sigma-Aldrich) and 1×PEST). Cells were treated in starvation medium using 5 μM estradiol (E2758, Sigma-Aldrich) and/or 5 μM 4-hydroxytamoxifen (Sigma-Aldrich) for 48 h before RNA isolation (RNeasy Mini Kit, 74106, Qiagen). EtOH was used as vehicle control, and treatment medium was replenished every 24 h. Samples prepared in quintuplicate individual repeats were checked for quality using a 2100 Bioanalyzer instrument (Agilent; RIN range, 9.6–10), used as templates to prepare libraries (TruSeq, Illumina), and subjected to RNA-seq analysis using a NextSeq instrument (Illumina). Raw sequencing data was demultiplexed and merged into two fastq files (read 1 and read 2) for each sample using Picard tools ExtractIlluminaBarcodes and IlluminaBasecallsToFastq (https://broadinstitute.github.io/picard/). Kallisto (v0.43.0)[62] was used for abundance estimation, and differential expression analysis was performed with Sleuth (v0.29.0)[63]. Kallisto was run with parameters '–bootstrap-samples 100', '–bias' and '–rf-stranded', and the transcript target was the Gencode release M15 protein-coding transcript sequences. The resulting lists of the top 1,000 differentially upregulated and 1,000 downregulated genes in *Pdgfc*$^{-/-}$ PeRo-Lum1 cells compared to *Pdgfc*$^{+/+}$ PeRo-Bas1 cells were used to investigate the enrichment of regulated genes with binding sites for the products of *ESR1*, *FOXA1* and *GATA3*, using publicly available data sets from ChIP–seq analyses. ChIP–seq data sets were obtained through the CistromeDB portal[64] and included E2-treated MCF-7 cells[30] (GSM589237, GSM659787 and GSM720422, respectively) and E2-treated T47D cells[30] (GSM589239, and GSM659795, respectively). ChIP–seq peaks were assigned to GRCh38 Ensembl gene transcripts (gencode_basic = TRUE, biotype = protein coding and miRNAs) and were scored using the ClosestGene method[65]. The ClosestGene method assigns a ChIP–seq peak to the closest transcription start site and scores the peak on the basis of the empirical cumulative distribution of peaks around the transcription start site. Transcript scores were summed on the gene level and used to examine the enrichment of binding in the top up- and downregulated genes observed in the experiment. From the human ChIP–seq data set, we extracted 15,140 genes that were homologous between human and mouse genomes using BiomaRt (filtering on ortholog_one2one, and homolog_orthology_confidence = 1). The ChIP–seq enrichment test was then confined to the intersection of genes with human and mouse homology and the 13,000 genes with detectable expression in the experiment (n = 11,300 genes). The summed score and the number of genes assigned to ChIP–seq peaks of the top 1,000 differentially expressed genes were compared to 100,000 lists of randomly sampled genes. The sampled gene lists were drawn from the pool of 11,300 genes to provide a relevant background. The number of bound genes and sum of scores in each resampled gene list was recorded and then ranked (the gene list with the highest score = rank 1) together with the results for the query lists. The rank of the query gene list divided by the total number of resample instances was then used as a P value for the probability to acquire the level of enrichment by chance.

For the analysis of gene expression in cell cultures following estradiol or tamoxifen treatment, we ranked all genes according to the Wald test statistic for differential expression. The Pearson's r correlation test was used to rank the genes that correlated with *PDGFC* expression within the TCGA breast carcinoma data set (BRCA). GSEA was performed using the GseaPreranked tool in GSEA v3.0 (refs. 66,67) with 1,000 random sample permutations and using the Molecular Signatures Database (MSigDB) hallmark (h.all.v6.1) and curated (c2.all.v6.1) gene sets. The GSEA statistics (normalized enrichment score (NES), nominal P value and FDR q value) are presented in the figures.

Statistical analyses. All values depicted represent mean ± s.e.m. Statistical calculations were performed using IBM SPSS Statistics (v22.0, IBM, Armonk, NY, USA) or GraphPad Prism 7 software. Statistical tests were applied as indicated in the figure legends in a two-sided, unpaired fashion, with $P < 0.05$ considered significant. The variance was similar between experimental groups in each experiment unless otherwise stated. *In vivo* experiments included cohorts of the size indicated in each figure legend but at least 6 mice per group. Sample size was chosen using an estimate of the number of mice needed to detect a 20% difference in the primary endpoint of tumor growth rate on the basis of the prior experience of the authors. No mice entering the experimental and/or intervention phase were excluded from analysis. *In vitro* analyses were repeated three to six times to ensure reproducible conclusions; the exact number of repetitions is stated in each figure legend.

Life Sciences Reporting Summary. Further information on experimental design is available in the **Life Sciences Reporting Summary**.

Data availability. Data from the transcriptional analysis of CAF2 cells stimulated with PDGF-CC is available through the NCBI GEO database with accession number GSE108835.

61. Parker, J.S. *et al.* Supervised risk predictor of breast cancer based on intrinsic subtypes. *J. Clin. Oncol.* **27**, 1160–1167 (2009).
62. Bray, N.L., Pimentel, H., Melsted, P. & Pachter, L. Near-optimal probabilistic RNA-seq quantification. *Nat. Biotechnol.* **34**, 525–527 (2016).
63. Pimentel, H. *et al.* Differential analysis of RNA-seq incorporating quantification uncertainty. *Nat. Methods* **14**, 687–690 (2017).
64. Mei, S. *et al.* Cistrome Data Browser: a data portal for ChIP–seq and chromatin accessibility data in human and mouse. *Nucleic Acids Res.* **45** D1, D658–D662 (2017).
65. Sikora-Wohlfeld, W., Ackermann, M., Christodoulou, E.G., Singaravelu, K. & Beyer, A. Assessing computational methods for transcription factor target gene identification based on ChIP–seq data. *PLOS Comput. Biol.* **9**, e1003342 (2013).
66. Subramanian, A. *et al.* Gene set enrichment analysis: a knowledge-based approach for interpreting genome-wide expression profiles. *Proc. Natl. Acad. Sci. USA* **102**, 15545–15550 (2005).
67. Mootha, V.K. *et al.* PGC-1α-responsive genes involved in oxidative phosphorylation are coordinately downregulated in human diabetes. *Nat. Genet.* **34**, 267–273 (2003).

doi:10.1038/nm.4494

nature research

Corresponding author(s): Kristian Pietras

Life Sciences Reporting Summary

Nature Research wishes to improve the reproducibility of the work that we publish. This form is intended for publication with all accepted life science papers and provides structure for consistency and transparency in reporting. Every life science submission will use this form; some list items might not apply to an individual manuscript, but all fields must be completed for clarity.

For further information on the points included in this form, see Reporting Life Sciences Research. For further information on Nature Research policies, including our data availability policy, see Authors & Referees and the Editorial Policy Checklist.

Please do not complete any field with "not applicable" or n/a. Refer to the help text for what text to use if an item is not relevant to your study.
For final submission: please carefully check your responses for accuracy; you will not be able to make changes later.

Experimental design

1. Sample size

Describe how sample size was determined.

See paragraph on Statistical analyses in section Online Methods

2. Data exclusions

Describe any data exclusions.

No animals were excluded from the analysis. See paragraph on Statistical analyses in section Online Methods

3. Replication

Describe the measures taken to verify the reproducibility of the experimental findings.

Experiments not involving animals were repeated at least three times to ensure reproducibility. For ethical reasons, only key experiments involving animals were replicated. All attempts at replication were successful. In the few cases were replication was not attempted, robust statistical analyses were applied to ensure that the results were scientifically valid

4. Randomization

Describe how samples/organisms/participants were allocated into experimental groups.

See paragraph on Animal experiments in section Online Methods

5. Blinding

Describe whether the investigators were blinded to group allocation during data collection and/or analysis.

Tumor size measurements in therapeutic trials were performed in a blinded fashion. Also, quantification of tumor parameters by histological analyses was performed in a blinded fashion.

Note: all in vivo studies must report how sample size was determined and whether blinding and randomization were used.

6. Statistical parameters

For all figures and tables that use statistical methods, confirm that the following items are present in relevant figure legends (or in the Methods section if additional space is needed).

n/a	Confirmed
☐	☒ The exact sample size (*n*) for each experimental group/condition, given as a discrete number and unit of measurement (animals, litters, cultures, etc.)
☐	☒ A description of how samples were collected, noting whether measurements were taken from distinct samples or whether the same sample was measured repeatedly
☐	☒ A statement indicating how many times each experiment was replicated
☐	☒ The statistical test(s) used and whether they are one- or two-sided *Only common tests should be described solely by name; describe more complex techniques in the Methods section.*
☐	☒ A description of any assumptions or corrections, such as an adjustment for multiple comparisons
☐	☒ Test values indicating whether an effect is present *Provide confidence intervals or give results of significance tests (e.g. P values) as exact values whenever appropriate and with effect sizes noted.*
☐	☒ A clear description of statistics including central tendency (e.g. median, mean) and variation (e.g. standard deviation, interquartile range)
☐	☒ Clearly defined error bars in all relevant figure captions (with explicit mention of central tendency and variation)

See the web collection on statistics for biologists for further resources and guidance.

Nature Medicine: doi:10.1038/nm.4494

Software

Policy information about availability of computer code

7. Software

Describe the software used to analyze the data in this study.	Statistical analyses were performed using GraphPad Prism 7 or SPSS version 22.0.

For manuscripts utilizing custom algorithms or software that are central to the paper but not yet described in the published literature, software must be made available to editors and reviewers upon request. We strongly encourage code deposition in a community repository (e.g. GitHub). *Nature Methods* guidance for providing algorithms and software for publication provides further information on this topic.

Materials and reagents

Policy information about availability of materials

8. Materials availability

Indicate whether there are restrictions on availability of unique materials or if these materials are only available for distribution by a third party.	All unique materials are readily available from the authors.

9. Antibodies

Describe the antibodies used and how they were validated for use in the system under study (i.e. assay and species).	STC1, Santa Cruz Biotechnologies, sc-30183, http://datasheets.scbt.com/sc-30183.pdf HGF, Abcam, ab83760, http://www.abcam.com/hgf-antibody-ab83760.html IGFBP3, Santa Cruz Biotechnologies, sc-9028, http://datasheets.scbt.com/sc-9028.pdf PDGFRA, eBioscience/ThermoFisher, 12-1401, https://www.thermofisher.com/order/genome-database/generatePdf?productName=CD140a%20(PDGFRA)&assayType=PRANT&detailed=true&productId=12-1401-81 PDGFRB, Cell Signaling, 3169S, https://media.cellsignal.com/pdf/3169.pdf ERa, DAKO, clone 1D5, https://www.thermofisher.com/order/genome-database/generatePdf?productName=Estrogen%20Receptor%20alpha&assayType=PRANT&detailed=true&productId=MA5-13191 ERa, Santa Cruz Biotechnology, sc-542, https://datasheets.scbt.com/sc-542.pdf FoxA1, Santa Cruz Biotechnology, sc-6553, http://datasheets.scbt.com/sc-6553.pdf B-actin, Abcam, ab-8227, http://www.abcam.com/beta-Actin-antibody-ab8227.pdf

10. Eukaryotic cell lines

a. State the source of each eukaryotic cell line used.	Cell lines were acquired from ATCC or established as primary mass cultures in house.
b. Describe the method of cell line authentication used.	Authentication was performed using fingerprinting on a regular basis.
c. Report whether the cell lines were tested for mycoplasma contamination.	All cell lines were confirmed negative for mycoplasma on a regular basis.
d. If any of the cell lines used are listed in the database of commonly misidentified cell lines maintained by ICLAC, provide a scientific rationale for their use.	NA

Animals and human research participants

Policy information about studies involving animals; when reporting animal research, follow the ARRIVE guidelines

11. Description of research animals

Provide all relevant details on animals and/or animal-derived materials used in the study.	See paragraph on Animals and Animal experiments in section Online Methods.

Policy information about studies involving human research participants

12. Description of human research participants

Describe the covariate-relevant population characteristics of the human research participants.	All patient cohort characteristics are supplied in Supplemental Table 1 and 3 of the manuscript.

Nature Medicine: doi:10.1038/nm.4494